TITLE PAGE

ENGINEERING DEVELOPMENT OF SLURRY BUBBLE COLUMN REACTOR (SBCR) TECHNOLOGY

Quarterly Technical Progress Report No. 24
For the Period 1 January – 31 March 2001

FINAL

Prepared by
AIR PRODUCTS AND CHEMICALS, INC.
7201 Hamilton Blvd.
Allentown, PA 18195-1501

Bernard A. Toseland, Ph.D.
Program Manager and Principal Investigator

Robert M. Kornosky
Contracting Officer's Representative

for the United States Department of Energy
Under Cooperative Agreement No. DE-FC22-95PC95051
Performance Period 3 April 1995 – 31 March 2002

DISCLAIMER

Comprehensive Table of Contents

ENGINEERING DEVELOPMENT OF SLURRY BUBBLE COLUMN REACTOR (SBCR) TECHNOLOGY

Quarterly Technical Progress Report No. 24
For the Period 1 January – 31 March 2001

Project Objectives

The major technical objectives of this program are threefold: 1) to develop the design tools and a fundamental understanding of the fluid dynamics of a slurry bubble column reactor to maximize reactor productivity, 2) to develop the mathematical reactor design models and gain an understanding of the hydrodynamic fundamentals under industrially relevant process conditions, and 3) to develop an understanding of the hydrodynamics and their interaction with the chemistries occurring in the bubble column reactor. Successful completion of these objectives will permit more efficient usage of the reactor column and tighter design criteria, increase overall reactor efficiency, and ensure a design that leads to stable reactor behavior when scaling up to large diameter reactors.

Abstract

Washington University's work for the quarter involved the study of the dynamic simulations of bubble columns in three dimensions. Work was also done in dynamic simulations of two-phase transient flow using CFDLIB. Ohio State measured the axial dispersion coefficients of the liquid phase. The steady-state thermal dispersion method was used to obtain the measurements. Iowa State followed the last quarter's work by using CFDLIB to simulate conditions described in the literature, with the objective of validating the simulation result. The group's work also led to a determination of the adequacy of periodic boundary conditions in representing small columns.

Executive Summary

In the twenty-fourth quarter's work, Washington University's team studied three-dimensional dynamic simulations of bubble columns. Numerical simulation was utilized to capture the significant features of column flows. Washington University also reported completion of 3D dynamic simulations for three sizes of bubble columns operating at different superficial gas velocities. The simulations were performed in CFDLIB, which was developed by the Los Alamos labs. The predicted overall gas holdup in each case was in good agreement with the experimentally measured value. Numerical liquid-phase particle tracking simulations covering columns of two different sizes were performed using CFDLIB. Numerically predicted axial diffusivities agreed well with the measured values calculated from CARPT data.

Ohio State measured the axial dispersion coefficients of the liquid phase in high-pressure columns by the steady-state thermal dispersion method. It was found that the axial temperature distribution in terms of $\ln[(T-T_0)/(T_m-T_0)]$ is almost linear at various gas velocities. The axial dispersion coefficient increases significantly with increasing gas velocity. The effect of liquid velocity on the axial liquid mixing is small compared to the effect of gas velocity. Ohio State also initiated the study of flow fields and Reynolds stresses at high pressures using a two-dimensional laser Doppler velocimetry (LDV) system calibrated under ambient conditions. In addition, Ohio State measured the axial liquid velocity profiles at different gas velocities under ambient conditions for the air-water system using the LDV technique. The regime transition was identified based on the liquid velocity measurement, and the transition superficial gas velocity obtained was about 4 - 6 cm/s in the air-water system.

Iowa State used 3D CFDLIB in simulating conditions described in the literature. In order to improve the resolution obtained through the first set of simulations, a second set was performed under the same conditions as the first, but with a smaller grid. This produced a high-resolution set of 3D simulations that the Iowa State group expects to be of great value in the work ahead.

WASHINGTON UNIVERSITY IN ST. LOUIS

The report for Washington University for the period follows.

ENGINEERING DEVELOPMENT OF SLURRY BUBBLE COLUMN REACTOR (SCBR) TECHNOLOGY

Twenty-Fourth Quarterly Report
for
January 1 – March 31, 2001

(Budget Year 6: October 1, 2000 – September 30, 2001)

Chemical Reaction Engineering Laboratory (CREL)
Chemical Engineering Department
Washington University

Objectives for the Sixth Budget Year

The main goal of this subcontract is to study the fluid dynamics of slurry bubble columns and address issues related to scaleup and design. The objectives set for the sixth budget year (October 1, 2000 – September 30, 2001) are listed below.

- Extension of CARPT database to high superficial gas velocity in bubble columns.
- Extension of the CARPT/CT database to gas-liquid-solid systems at high superficial gas velocity.
- Evaluation of the effect of sparger design on the fluid dynamics of bubble columns using the CARPT technique.
- Interpretation of LaPorte tracer data.
- Further improvement in Computational Fluid Dynamics (CFD) using CFDLIB and Fluent.

In this report, the research progress and achievements accomplished in the twenty-fourth quarter (January 1, 2001 – March 31, 2001) are summarized.

HIGHLIGHTS FOR THE 24th QUARTER

1. Three-Dimensional Dynamic Simulation of Bubble Columns

- Three-dimensional dynamic simulations of two-phase (air/water) transient flow in cylindrical bubble columns were performed using CFDLIB.
- The key dynamic features of bubble column flows -- consisting of a tornado-like upward spiral liquid motion, pushed by a high volume of gas that sweeps across the core region, and the downward liquid gulf stream within the wall region -- were captured by numerical simulation.
- The time-averaged liquid velocity vector plots compared well with the CARPT measurements of Degaleesan (1997).

2. Mean Axial Liquid Velocity Profiles – Numerical versus CARPT

- Three-dimensional dynamic simulations of two-phase (air/water) transient flow in cylindrical bubble columns were performed using CFDLIB. The simulations covered columns of three different diameters (6, 8 and 18 in.) operated at various superficial gas velocities (2 to 12 cm/s).
- The predicted overall gas holdup in each case was in good agreement with the experimentally measured value.
- The time-averaged radial profiles of the liquid axial velocity compared well with the CARPT data of Degaleesan (1997) in the 6- and 8-in. diameter column. However, there were discrepancies in the predicted inversion point and velocity profile shape for the 18-in. diameter column.

3. Evaluation of Turbulent Eddy Diffusivity in Bubble Columns by Numerical Particle Tracking

- Numerical liquid-phase particle tracking simulations were performed using CFDLIB. The simulations covered columns of two different sizes (8- and 18-in. diameters) operated at superficial gas velocities of 12 and 10 cm/s, respectively.
- The Lagrangian turbulent eddy diffusivity for the liquid phase was evaluated using the numerically tracked particle trajectories and compared with the corresponding values calculated from CARPT data.
- The numerically predicted axial diffusivities agreed well with the measured values; the agreement for the azimuthal diffusivities was less impressive, while the values for the radial diffusivities were significantly under-predicted.

1. Three-Dimensional Dynamic Simulation of Bubble Columns

1.1 Introduction

It is widely recognized that the physical models used in the current numerical investigations, which include the inter-phase momentum exchange models and multiphase turbulence models, require experimental data for verification and improvement. Three-dimensional dynamic simulations of the highly transient gas-liquid flow in either cylindrical or rectangular bubble columns are needed.

In this study we present a Eulerian/Eulerian dynamic simulation of a three-dimensional gas-liquid bubble column using the Los Alamos finite-volume multiphase flow simulation library, CFDLIB. We focus on the comparisons with the experiments of Degaleesan (1997), who studied the fluid dynamics of bubble columns by using the Computer Automated Radioactive Particle Tracking (CARPT) technique in our laboratory.

For the purpose of the present simulations, we have modified some parts of the code related to the inter-phase momentum exchange and turbulence calculations. For the drag coefficient, C_D, we use the following expression (Drew 1983):

$$C_D = max\left[\frac{24}{Re}\left(1 + 0.15\,Re^{0.687}\right),\, f\,\frac{8}{3}\frac{Eo}{Eo+4}\right] \tag{1.1}$$

in which

$$f = \left\{\frac{1+17.67(1-\varepsilon)^{9/7}}{18.67(1-\varepsilon)^{3/2}}\right\}^2 \tag{1.2}$$

The Eotvos number, Eo, and bubble Reynolds number, Re, are defined as

$$Eo \equiv E\, g\rho_c d_p^2 \big/ \gamma \tag{1.3}$$

And

$$\mathrm{Re} \equiv d_b \left|\mathbf{u}_l - \mathbf{u}_g\right| \big/ \upsilon_l \tag{1.4}$$

In the momentum equation for the liquid phase, we adopted a model for the bubble-induced stress, as proposed by Sato *et al.* (1981):

$$\sigma_c^b = \rho_c \nu_b^t (\nabla \mathbf{u}_l + \nabla \mathbf{u}_l^T) \tag{1.5}$$

in which the bubble-induced additional viscosity is calculated by

$$\nu_b^t = k_b \varepsilon d_b \left|\mathbf{u}_l - \mathbf{u}_g\right| \tag{1.6}$$

The empirical constant k_b takes a value from 0.2 to 0.6, and is taken as 0.4 in this simulation.

1.2 Results and Discussion

All simulations start from a static initial condition where the main body of the column is filled with water and the top part only with gas. Figure 1.1 shows a typical mesh system

used for a cylindrical column. CFDLIB requires a structured mesh system consisting of logical cubic cells. At the cross-sectional plane (x-y plane), the elliptically smoothed, body-fitted mesh is used. In the axial direction (z-direction), the grid is uniform. In order to obtain a better comparison with experimental data, we set the conditions for our simulations as close to those in Degaleesan's (1997) experiment as possible. Initially the column is filled with liquid (water), i.e., $\varepsilon_l = 1;\ \varepsilon_g = 0,$ up to the level that matches the static liquid height in the experiment. Above this level, the initial condition is $\varepsilon_l = 0;$ $\varepsilon_g = 1$. To prevent liquid flooding from the column, the computational domain in the axial direction is about 50 to 80% higher than the static liquid height. The gas is introduced at the bottom of the column, and only gas is allowed to cross the bottom boundary. Since it is very difficult and not necessary to resolve the gas injectors used in the experiments (e.g., 0.5-1.0-mm-diameter holes on perforated plate) with the currently employed mesh, the gas is introduced uniformly over the bottom plane. For the gas phase, the free-slip boundary condition is imposed on the column's wall. For the liquid phase, since the thin boundary layer cannot be resolved, either the free-slip or the no-slip condition can be used. Finally, the pressure condition, i.e., the atmospheric pressure $p = 0$, is imposed on the top of the column.

The gas-liquid flow in bubble columns is highly transient and turbulent. Figure 1.2 shows the instantaneous iso-surfaces of the gas volume fraction in columns of different diameters operated at different superficial gas velocities. The plots show the three-dimensional spiral structures and transient pockets of high gas volume fraction mixtures rising up in a continuous fashion. Figure 1.3 shows the instantaneous contour plot of gas holdup on a central ($r - z$) plane of the 44-cm diameter column operated at 2, 5 and 10 cm/s superficial gas velocities. Here we see that the free surface, i.e., the dynamic height of the gas-liquid mixture in the column, rises as the superficial gas velocity increases. The turbulent character of the flow can be further observed by looking at the instantaneous velocity fields. Figure 1.4 shows the instantaneous liquid velocity vectors projected on a ($r - z$) plane (at $\theta = 0$) of the 44-cm diameter column. One can clearly see the spiral structures associated with the transient eddies. Figure 1.5 shows the snapshots of liquid velocity vectors on cross-sectional ($x - y$) planes located at the top, middle and bottom regions of the column. The vortices are observed in the middle and bottom sections. At the upper end of the column, the gas disengagement zone, as shown in Figure 1.5(a), resembles a fountain-like pattern. In Figure 1.6, we exhibit the correlation between liquid velocity and gas holdup. Figure 1.6(a) is the top view of the instantaneous liquid velocity vector (3D) plot, on a cross-sectional plane located at the middle section, overlapped by the gas holdup contour plot on the same plane. The flow visualization package used does not allow the display of negative velocities. We notice that the upward rising vortices ($u_z > 0$) are associated with the high gas holdup pockets, as indicated by the dark areas in Figure 1.6(a). By comparing Figure 1.6(a) with Figure 1.6(b), in which only the liquid velocity vectors are plotted, we see that all the vortices are accompanied by upwards motion, and the non-vortical areas are in downwards motion. Hence, as shown in Figures 1.2-1.6, our simulations reveal the dynamic features of bubble columns -- tornado-like upward spiral liquid motion pushed by a high volume of gas that sweeps across the core region and the downwards liquid gulf stream within the

wall region. It is such spiral motions that push the gas towards the center of the column, resulting in the non-uniform radial distribution of gas holdup. It should be noted that the visualizations shown in Figures 1.2-1.6 are chosen at random, in time and/or in space, from the simulations. Due to the turbulent/transient nature of the flows, the exact time and location of these plots are obviously not relevant to the qualitative observations.

Figure 1.7 shows the longitudinal sections (side view) of the time-averaged liquid velocity vector plots for the 14-cm diameter column. The angle between the longitudinal planes is $\pi/4$. The choice of these planes is arbitrary. Spanning the entire column, the single-cell circulation flow pattern is clearly seen from various side views, as observed experimentally by Devanathan (1991) and Degaleesan (1997). In addition, the flow pattern is reasonably symmetric with respect to the column axis. From a height of about one column diameter, D_c, above the distributor, the flow appears to be quite well developed, with negligible radial and angular velocities.

Figure 1.8 shows the cross-sectional views of the time-averaged liquid velocity vectors for the same cases shown in Figure 1.7. At the upper end of the column, near the disengagement zone, the flow reversal is symmetric about the column axis, as shown by the upper plot of Figure 1.8, resembling a fountain like pattern with negligible angular velocity component. In the middle section, both the radial and angular time-averaged velocity components are negligibly small. This indicates that time-averaged liquid velocity in the middle section of the column is nearly one-dimensional, i.e. unidirectional with radial dependency only. At the bottom of the column, shown by the lower plot of Figure 1.8, the inwards flow pattern is the result of liquid descending along the column wall. All of these cross-sectional views of the time-averaged liquid velocity vectors compare well with CARPT measurements (Degaleesan, 1997).

2. Mean Axial Liquid Velocity Profiles – Numerical versus CARPT

2.1 Introduction

We have completed the three-dimensional dynamic simulations for three sizes of bubble columns operated at different superficial gas velocities. The conditions used in the simulations were the same as those employed in the CARPT experiments performed in our laboratory. The diameters of the columns and the operating conditions, i.e., the superficial gas velocity, for each case are listed in Table 2.1. The cases studied cover flow regimes ranging from bubbly flow to churn turbulent flow. The objective was to validate the numerical results by comparison with data, and further, to assess the capacity of the current two-fluid model to predict the fluid dynamics in bubble column reactors. In the present report we focus on the comparison of the mean axial liquid velocity.

CFDLIB, a package developed by the Los Alamos National Laboratory, was used for the simulations presented in this report. The modifications of part of the code related to the inter-phase momentum exchange and turbulence calculations and the numerical mesh system employed for our simulation were discussed in the previous report (October – December 2000).

2.2 Results and Discussion

All simulations start from a static initial condition in which the main body of the column is filled with water and the top part only with gas. The simulations are then performed until a quasi-steady state is reached. The time-averaged quantities are then calculated. In all simulations, the velocity and gas holdup fields are sampled every 0.05 - 0.1 seconds. To ensure the convergence of the averaged quantities, the averaging processes are performed for 50 - 80 seconds. The spatial averaging is then conducted along the vertical direction within the lower, middle and upper sections of the column.

The grid size and boundary conditions used are listed in Table 2.1. For each simulation, we first compared the overall global gas holdup, indicated by a column's dynamic height, with the experimental measurements, as listed in Table 2.1. The dynamic heights from the simulations were obtained by time-averaging the fluctuating interface level. The agreement between calculated and measured overall gas holdup was excellent (within a couple of percentage points), except at the highest gas velocity in the smallest diameter column.

Figure 2.1 shows the time- and azimuthally averaged axial liquid velocity profiles, $U_z(r)$, for a 14-cm diameter column at different superficial gas velocities. Some results for the 14-cm diameter column simulation were reported before. The compared profiles concerned the middle section of the column, where the mean flow could be assumed to be one-dimensional. For this relatively small diameter column, the simulation results at high U_g (9.6 and 12 cm/s) were in better agreement with the data than those at lower U_g (2.4 and 4.8 cm/s).

Figure 2.2 compares the numerically predicted radial distribution of the mean axial liquid velocity with experimental data in a 19-cm diameter column operated at 2, 5 and 12 cm/s superficial gas velocity. For these three cases, the numerical predictions agreed quite well with the data. The effect of using a different boundary condition on the wall can be seen by comparing the curves of the cases with no-slip condition (U_g=2 and 5 cm/s) with that of the free-slip condition (U_g=10 cm/s). The free-slip condition yielded better agreement with data in the near-wall region than did the no-slip condition. Obviously the boundary layer is too thin to be resolved by either measurement or simulation. For the gas-driven flow as found in bubble columns, the wall boundary is of less interest. Further, the wall friction is negligible in the global momentum balance. For these reasons, we consider the free-slip wall boundary condition appropriate for the cases of realistic superficial gas velocity, say U_g>10 cm/s.

Figure 2.3 compares the numerical mean velocity profiles with CARPT-measured profiles for the 44-cm diameter column operated at superficial gas velocities of 2, 5 and 10 cm/s. There are two noticeable differences between the calculated and the measured results. The inversion points, i.e., the radial location where U_z=0, for all the experimental profiles fall at $r/R \approx 0.68$, while those for the numerically predicted profiles move outwards to $r/R \approx 0.75$. This is an indication of the discrepancy in computed and actual

gas holdup profiles, i.e., the time-averaged radial distribution of gas holdup. We also notice that the experimental liquid velocity profiles for U_g=5 cm/s and 10 cm/s are fairly close. It seems that as U_g increases beyond a certain value, the liquid velocity does not linearly increase any more to the extent observed at lower U_g. Such behavior may indicate a transition from bubbly flow to churn turbulent flow where the mechanisms of bubble-bubble and bubble-liquid interactions are different. However, the model adopted in the current simulation is based on the assumption of single-size bubbles and neglects bubble-bubble interactions and therefore cannot account for such a change of mechanism. The possible transition, therefore, is not reflected in the numerical profiles shown in Figure 2.3. Further investigations of the reasons for the discrepancies between experimented and observed velocity profiles are in progress.

Table 1. Column Size, Operating Conditions and the Corresponding Computational Parameters

Column diameter D_c (cm)	Superficial gas velocity U_g (cm/s)	Static liquid height (cm)	Measured dynamic height (cm)	Measured overall gas holdup	Simulated dynamic height (cm)	Computed overall gas holdup	$\Delta x, \Delta y$ (cm)	Δz (cm)	Wall boundary condition
14	2.4	98	105	0.067	106	0.075	0.93	1.96	free-slip
	4.8	98	112	0.125	113	0.133	0.70	1.23	no-slip
	9.6	98	123	0.203	124	0.209	0.70	1.53	no-slip
	12	98	126	0.222	137	0.285	0.93	2.45	free-slip
19	2	104	115	0.093	110	0.054	1.1	2.1	no-slip
	5	104	128	0.191	123	0.154	1.1	2.1	no-slip
	12	96	124	0.230	130	0.262	1.1	1.9	free-slip
44	2	179	193	0.073	192	0.068	2.2	4.5	free-slip
	5	179	210	0.147	210	0.148	2.2	4.5	free-slip
	10	176	218	0.191	220	0.200	2.2	4.4	no-slip

3. Evaluation of Turbulent Eddy Diffusivity in Bubble Columns by Numerical Particle Tracking

3.1 Introduction

The dispersion of passive scalars by continuous motion in turbulent flows evolved as a major field of research, particularly during recent years. This evolution was due to industrial and environmental issues of utmost importance related to the energy crisis, spreading pollution and the need to improve plant design for two- or multi-phase flow processes. In the design of bubble column reactors, liquid phase mixing is one of the important factors that not only governs the residence time distribution of the liquid, but also affects that of the gas phase, and in addition, determines the mean driving force for mass transfer. As is well known, turbulence largely enhances the transport and mixing of any passive scalar released to a continuous material phase. The rates of transfer and mixing in the presence of turbulence are orders of magnitude larger than the rates due to molecular transport alone. The most common method of dealing with equations governing turbulent flow is treating the diffusive nature of turbulence via the introduction of a turbulent diffusivity for a given quantity. This is usually done using the gradient model, based on the well-known Boussinesq's hypothesis. With a suitable diffusivity, such a model appears in the averaged mass balance equation as a diffusive term. However, the turbulent eddy diffusivity that appears in the resulting equations is itself unknown and needs to be modeled.

While molecular diffusivity is caused by the Brownian motion of molecules, the turbulent eddy diffusivity is naturally related to the Lagrangian turbulent motion of fluid particles. Measurements and simulations of fluid particle velocities and trajectories, in a Lagrangian framework, are therefore needed for the study of the turbulent eddy diffusivity. The CARPT technique is capable of recording the Lagrangian trajectory of a tracer particle traveling through the entire column in a reasonable period of time. The Lagrangian turbulent eddy diffusivities are then directly evaluated from such data. Similarly, numerical particle tracking can be performed in a velocity field generated by the dynamic simulations of the transient gas-liquid flow in bubble columns. The numerical particle trajectories can then also be used to calculate the Lagrangian turbulent eddy diffusivities. In this sense there is no difference between the CARPT data and the data from numerical particle tracking.

However, there has been no generally established relationship between the eddy diffusivities, arising from the Boussinesq's gradient approximation, and the turbulent eddy diffusivities defined in the Lagrangian framework. In an isotropic and homogeneous turbulence field, it has been shown that the diffusivity appearing in the convection-diffusion equation can be approximated by the Lagrangian-based turbulent eddy diffusivities (Tenneke and Lumley, 1972). This is accomplished by using scale arguments and by comparing the probability distribution function for the spread of particles with the solution of the turbulent convective diffusion equation. Even without such a relation, the Lagrangian information deduced from a CARPT experiment directly reveals the characteristics of the dispersion process in the liquid phase and can be utilized

to study and model the effect of fluid dynamics on liquid-phase mixing in bubble columns.

In this report we evaluate the Lagrangian turbulent eddy diffusivity in bubble columns by utilizing numerical particle tracking. We compare the diffusivities from CARPT measurements with the ones from numerical simulation. Such comparison also serves as a validation of the numerical predictions arising from the two-fluid simulation of bubble column hydrodynamics.

3.2 Results and Discussion

As stated in the previous report (October – December 2000), we completed the three-dimensional dynamic simulations for bubble columns of three sizes operated at different superficial gas velocities and compared the time-averaged quantities with the data from CARPT experiments. From these simulations, we chose two cases for particle tracking simulation: a 44-cm diameter column operated at a superficial gas velocity of 10 cm/s and a 19-cm diameter column operated at U_g=12 cm/s. Both cases are within the churn turbulent flow regime, which is of interest to us. The simulations start from fully developed flow fields. Unlike the CARPT experiment, where the technique is able to follow a single tracer particle only, numerically there is no limit to the number of particles that can be traced simultaneously. Typically, 5000 initially randomly seeded particles are followed in a simulation. The dynamic simulation of the fluid flow field continues while the particle tracking is being performed. For the cases reported here, the simulation ran about 20 seconds, and the sampling frequency for the particle trajectory was 50 Hz, the same as in CARPT experiments, i.e., the position of the particle was recorded every 0.02 second. Figure 3.1 shows the trajectory of a numerical particle that was arbitrarily chosen from the 5000 particles, and the trajectory of the CARPT particle in the same column and under the same operating condition. The trajectory displayed represents 20 seconds from an arbitrary starting position.

For the general case, the turbulent eddy diffusivity is a second order tensor. In a Cartesian coordinate system, it is defined as

$$D_{ij}(\tau) \equiv \frac{1}{2}\frac{d}{d\tau}\overline{\{x_i(\tau+t)-x_i(t)\}\{x_i(\tau+t)-x_i(t)\}} \qquad (3.1)$$

where the over bar indicates the averaging over time t and different particles. In terms of cylindrical coordinates, each component of the diffusivity tensor is calculated as

$$D_{rr} = \overline{u_x \Delta x \cos^2\theta} + \overline{u_y \Delta y \sin^2\theta} + \overline{\cos\theta\sin\theta(u_y \Delta x + u_x \Delta y)} \qquad (3.2)$$

$$D_{\theta\theta} = \overline{u_x \Delta x \sin^2\theta} + \overline{u_y \Delta y \cos^2\theta} - \overline{\cos\theta\sin\theta(u_y \Delta x + u_x \Delta y)} \qquad (3.3)$$

$$D_{zz} = \overline{u_z' \Delta z'} \qquad (3.4)$$

$$D_{r\theta} = \overline{\left(u_x \Delta y + u_y \Delta x\right)\left(\cos^2\theta - \sin^2\theta\right)} + 2\overline{\sin\theta\cos\theta\left(u_y \Delta y - u_x \Delta x\right)} \tag{3.5}$$

$$D_{rz} = \overline{\left(u_x \Delta z' + u_z' \Delta x\right)\cos\theta} + \overline{\left(u_y \Delta z' + u_z' \Delta y\right)\sin\theta} \tag{3.6}$$

$$D_{\theta z} = \overline{\left(u_y \Delta z' + u_z' \Delta y\right)\cos\theta} - \overline{\left(u_x \Delta z' + u_z' \Delta x\right)\sin\theta} \tag{3.7}$$

in which

$$\Delta x = x(\tau + t) - x(t); \qquad \Delta y = y(\tau + t) - y(t); \qquad \Delta z' = z'(\tau + t) - z'(t);$$

$$u_x = u_x(\tau + t); \qquad u_y = u_y(\tau + t); \qquad u_z' = u_z'(\tau + t)$$

$$\cos\theta = \frac{x(\tau + t)}{\sqrt{x^2(\tau + t) + y^2(\tau + t)}}; \qquad \sin\theta = \frac{y(\tau + t)}{\sqrt{x^2(\tau + t) + y^2(\tau + t)}};$$

Here we need to exclude the effect of convection due the mean axial velocity, $U_z(r)$, by using

$$u_z'(\tau + t) = u_z(\tau + t) - U_z[r(t + \tau)]; \quad r = \sqrt{x^2(t + \tau) + y^2(t + \tau)}; \tag{3.8}$$

for the fluctuating velocity in axial direction and

$$z'(t) = \int_0^t u_z'(s)ds \tag{3.9}$$

for the displacement in axial direction caused by the above fluctuating velocity only.

Figure 3.2 compares the numerical values of D_{zz}, D_{rr} and $D_{\theta\theta}$ with those evaluated from CARPT data for the 44-cm-diameter column operated at a superficial gas velocity of 10 cm/s. Figure 3.3 shows the same comparison for the 19-cm-diameter column operated at a superficial gas velocity of 12 cm/s. For both cases, the numerical simulation predicted the axial diffusivity, D_{zz}, quite satisfactorily. However, the simulations under-predicted the peak values of the radial diffusivity, D_{rr}, by about 100%. Asymptotically, the numerical radial diffusivity approached zero, while the experimental radial diffusivity approached finite values. The reasons for this discrepancy will be studied in the future. The numerically predicted azimuthal diffusivities, $D_{\theta\theta}$, behaved similarly to the measured values. As stated earlier, one of the objectives of evaluating the Lagrangian turbulent eddy diffusivities is to determine whether these diffusivities are appropriate terms to use in the gradient diffusion model. From a practical point of view, most proposed models are either 1D or 2D, such as the axial dispersion model (ADM)

and the recycle and cross flow with dispersion (RCFD) model (Degaleesan, 1997). Only the radial and axial eddy diffusivities are therefore of interest. For an axial dispersion model, one needs the axial eddy diffusivity and the mean liquid velocity, i.e., the liquid re-circulation, profile to evaluate the dispersion coefficient, as shown by Degaleesan and Dudukovic (1998). We have shown here that the 3D dynamic simulations can provide such information with reasonable accuracy.

Future Work

Estimating the local interfacial area has been derived from the overall gas holdup estimate, assuming mean bubble size. Estimating this interfacial area provides one of the most important bubble column reactor modeling parameters. In a recent development, local interfacial area was calculated locally, based upon predicted local gas holdup and assumed mean bubble size in current CFD simulation.

In its next report, Washington University expects to introduce the bubble population balance equation that has been deemed necessary to the attainment of better and more accurate estimates.

References

Degaleesan, S., "Fluid dynamic measurements and modeling of liquid mixing in bubble columns," D. Sc. Thesis, Washington University in St. Louis (1997).

Degaleesan, S. and M. P. Dudukovic, "Liquid backmixing in bubble columns and the axial dispersion model," *AICHE J*., **44**(11), 2369-2378 (1998).

Devanathan, N., "Investigation of liquid hydrodynamics in bubble columns via computer automated radioactive particle tracking (CARPT)," D. Sc. Thesis, Washington University in St. Louis (1991).

Drew, D. A., "Mathematical modeling of two-phase flow", *Ann. Rev. Fluid Mech*., 15, 261 (1983).

Sato, Y., M. Sadatomi and K. Sekoguchi, "Momentum and heat transfer in two-phase bubble flow I," *Int. J. Multiphase Flow*, 7, 167 (1981).

Tennekes, H. and J. L. Lumley, "A first course in turbulence," The MIT Press, Cambridge, Massachusetts, USA (1972)

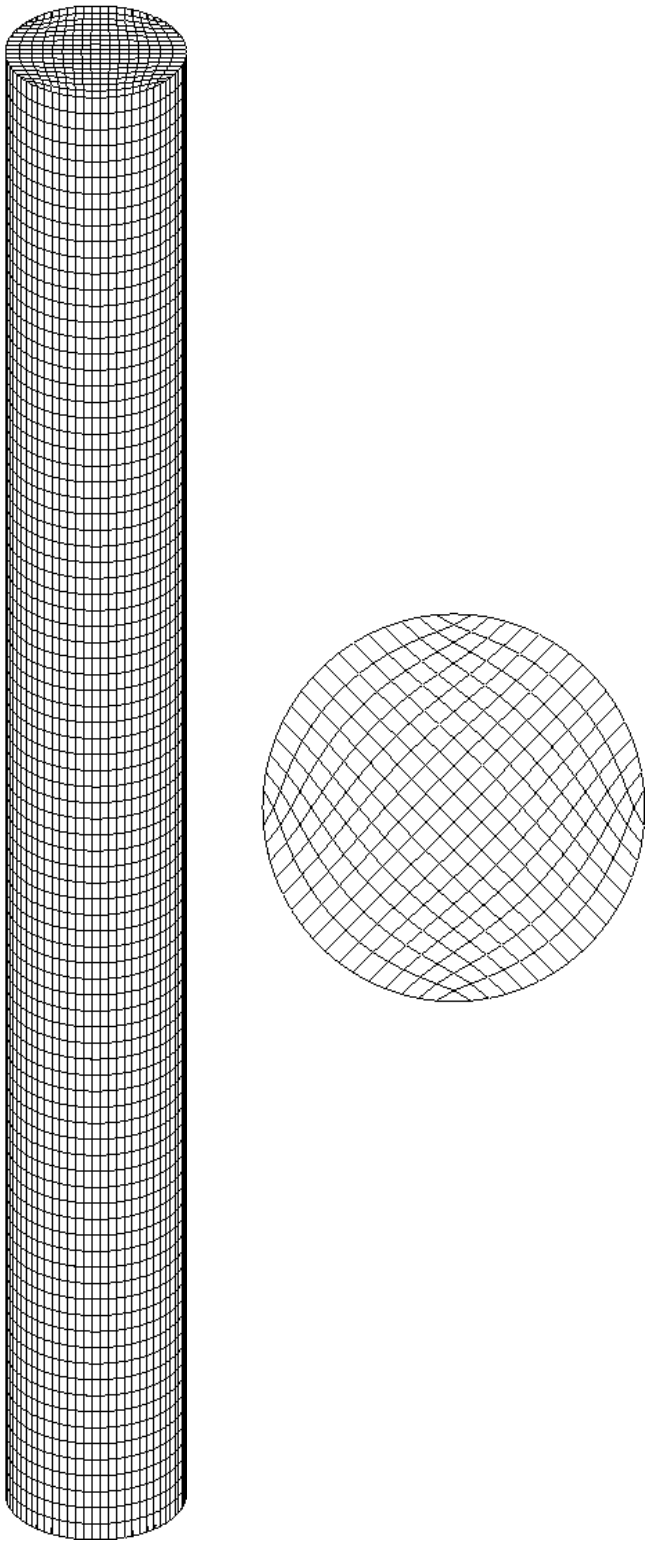

Figure 1.1 Computational Meshes

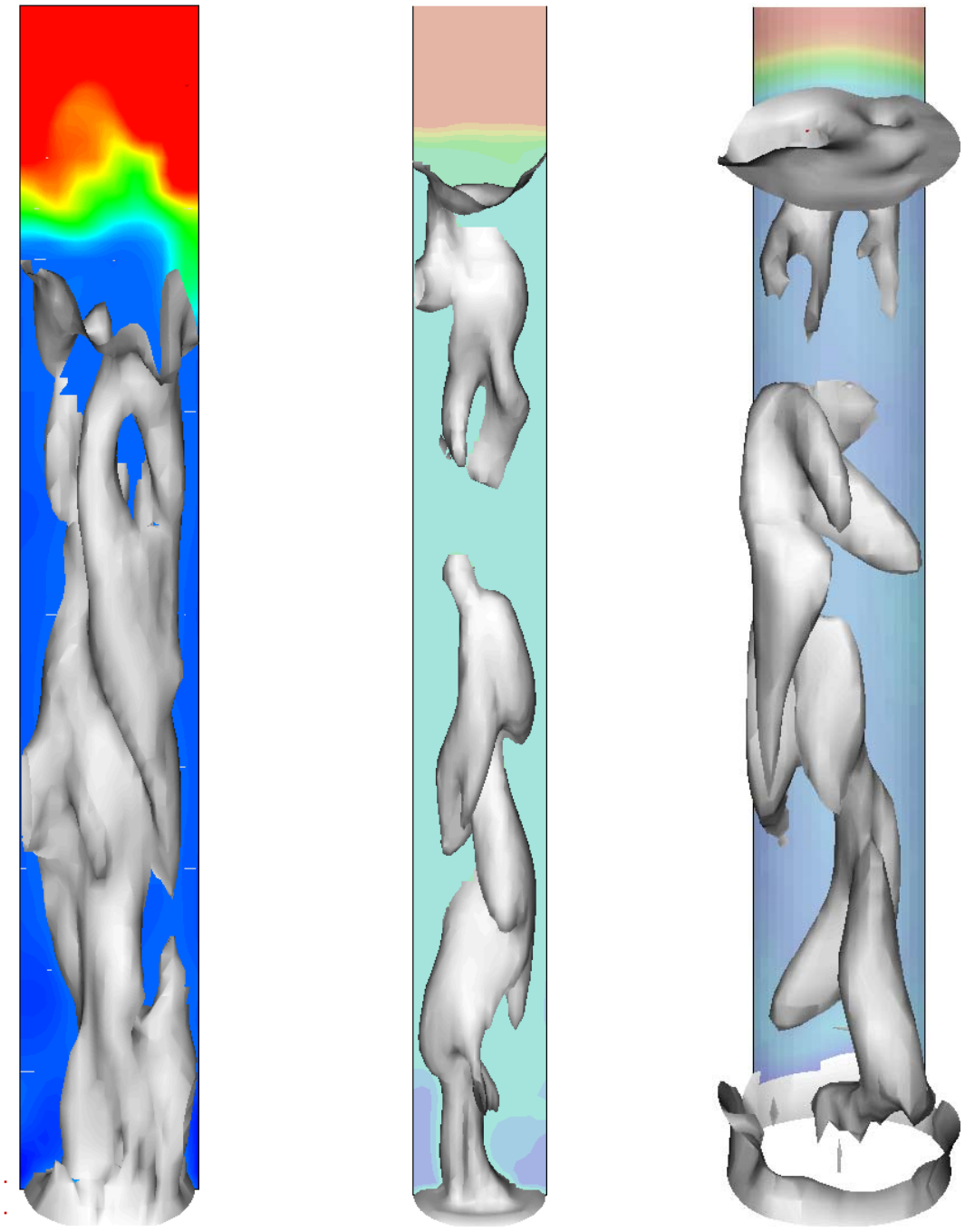

(a) (b) (c)

Figure 1.2 The Instantaneous Iso-Surface of the Gas Holdup, ε_g, in Various Bubble Columns: (a) D_c = 19cm; U_g = 2cm/s; ε_g = 0.08 (b) D_c = 14cm; U_g = 9.6cm/s; ε_g =0.33 (c) D_c = 44cm; U_g = 10cm/s; ε_g =0.28

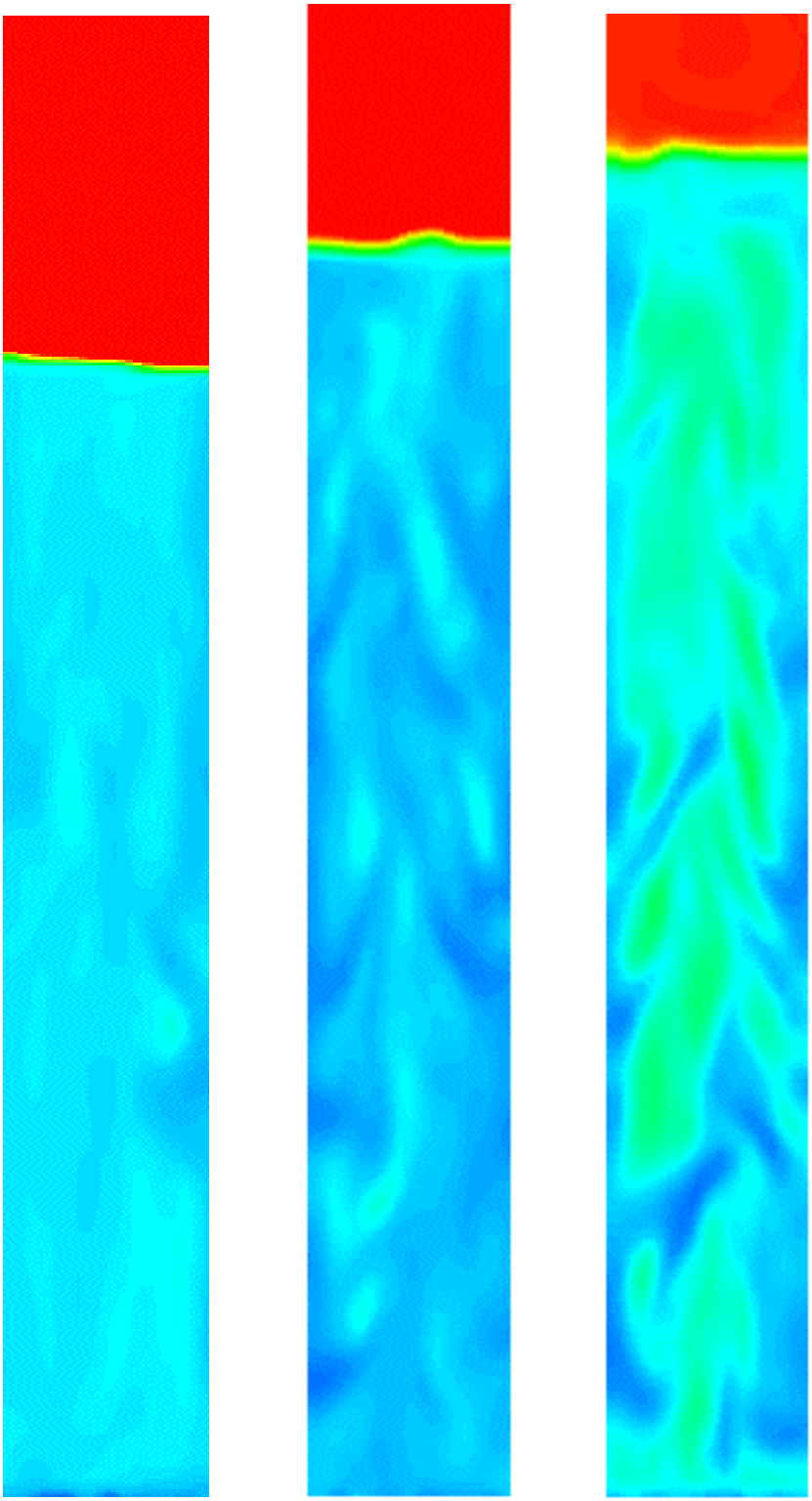

(1) 2cm/sec (2) 5cm/sec (3) 10cm/sec

Figure 1.3 Contour Plot of the Instantaneous Gas Holdup on a Plane Slice through the Center of a 44-cm Diameter Column Operated at Different Superficial Gas Velocities

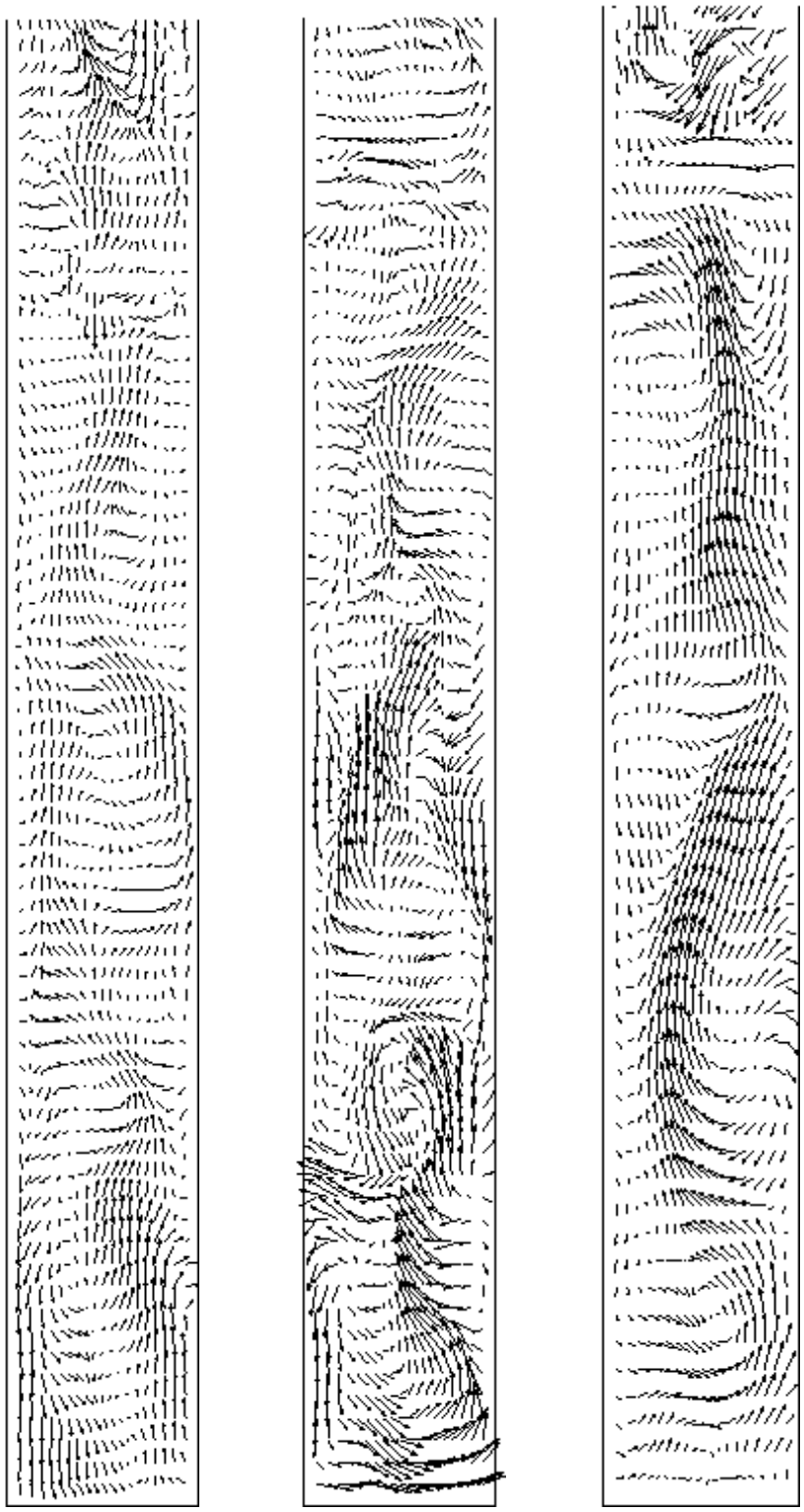

(1) 2 cm/s; (2) 5 cm/s; (3) 10 cm/s

Figure 1.4 The Vector Plot of the Instantaneous Liquid Velocity Projected on a r-z Plane Slice through the Center of a 44-cm Diameter Column Operated at Different Superficial Gas Velocities

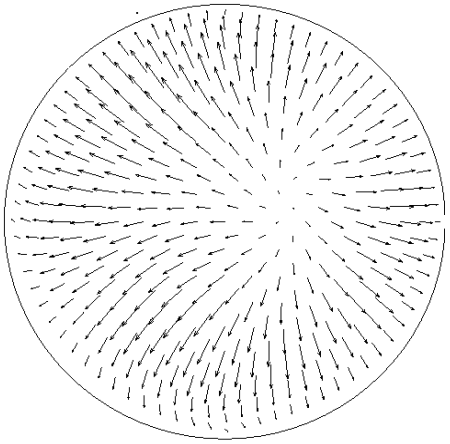

(a) Upper section

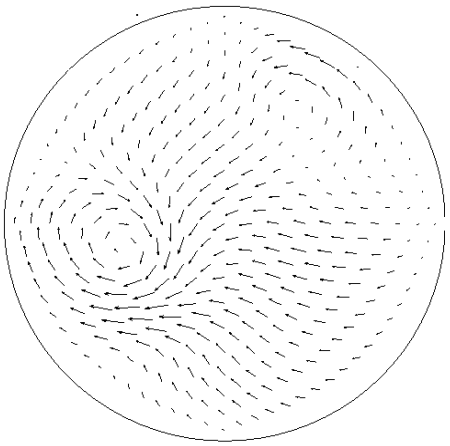

(b) Middle section

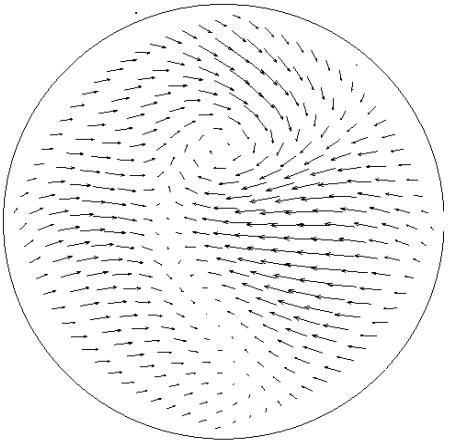

(c) Bottom section

Figure 1.5 The Vector Plots of the Instantaneous Liquid Velocity Projected on Cross-Sectional (x-y) Planes of a 44-cm Diameter Column Operated at a Superficial Gas Velocity of 10 cm/s

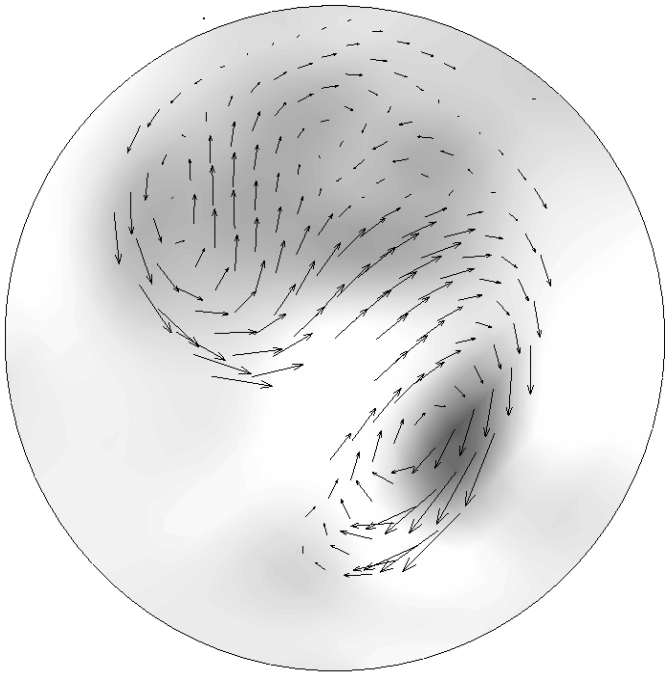

(a) Gas holdup and liquid velocity

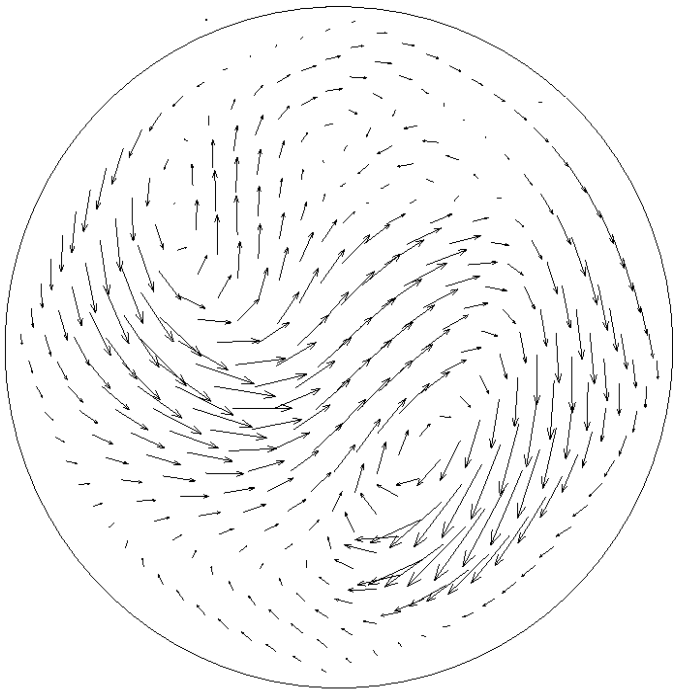

(b) Liquid velocity

Figure 1.6 The Instantaneous Flow Pattern on a Cross-Sectional Plane of a 44-cm Diameter Column Operated at a Superficial Gas Velocity of 10 cm/s

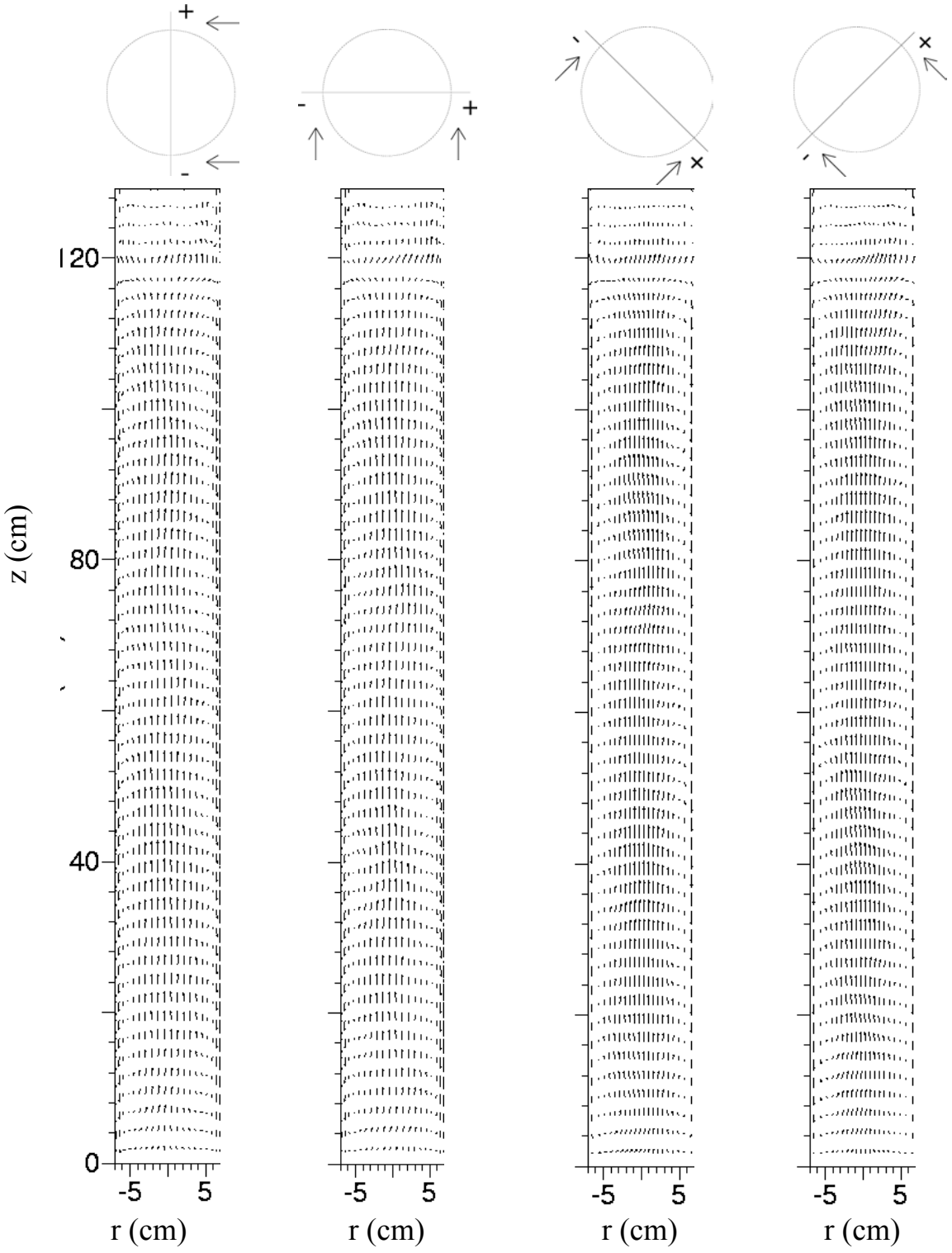

Figure 1.7 Time-Averaged Liquid-Velocity Vectors on Planes Cutting through the Center of the 14-cm Diameter Column Operated at a Superficial Gas Velocity of 4.8 cm/s

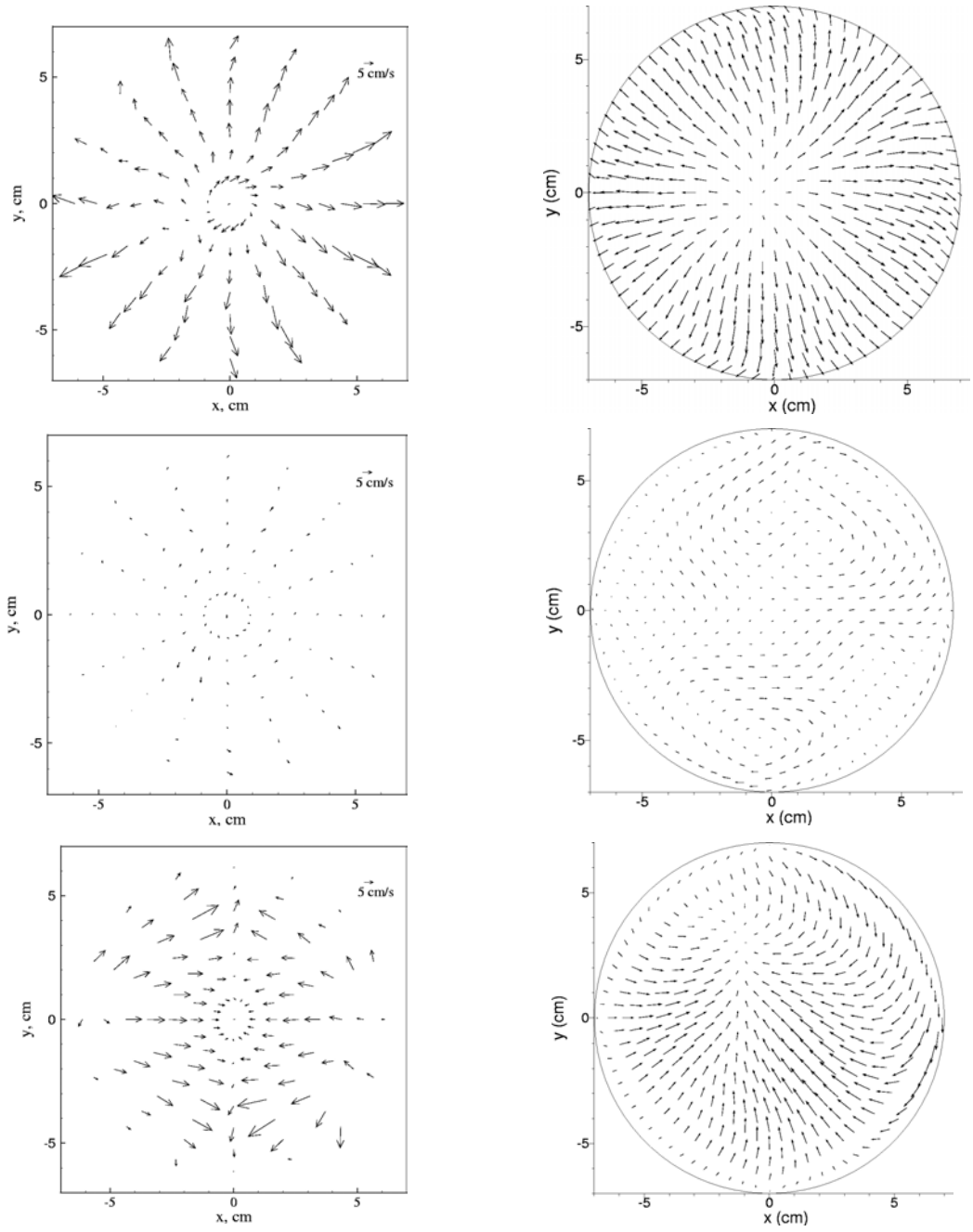

Figure 1.8 Comparison of Time-Averaged Liquid-Velocity Vectors on Cross-Sectional Planes at the Gas Sparger Zone (lower row), the Middle Section (middle row) and the Gas Disengagement Zone (upper row) of a 14-cm Diameter Column at 4.8 cm/s

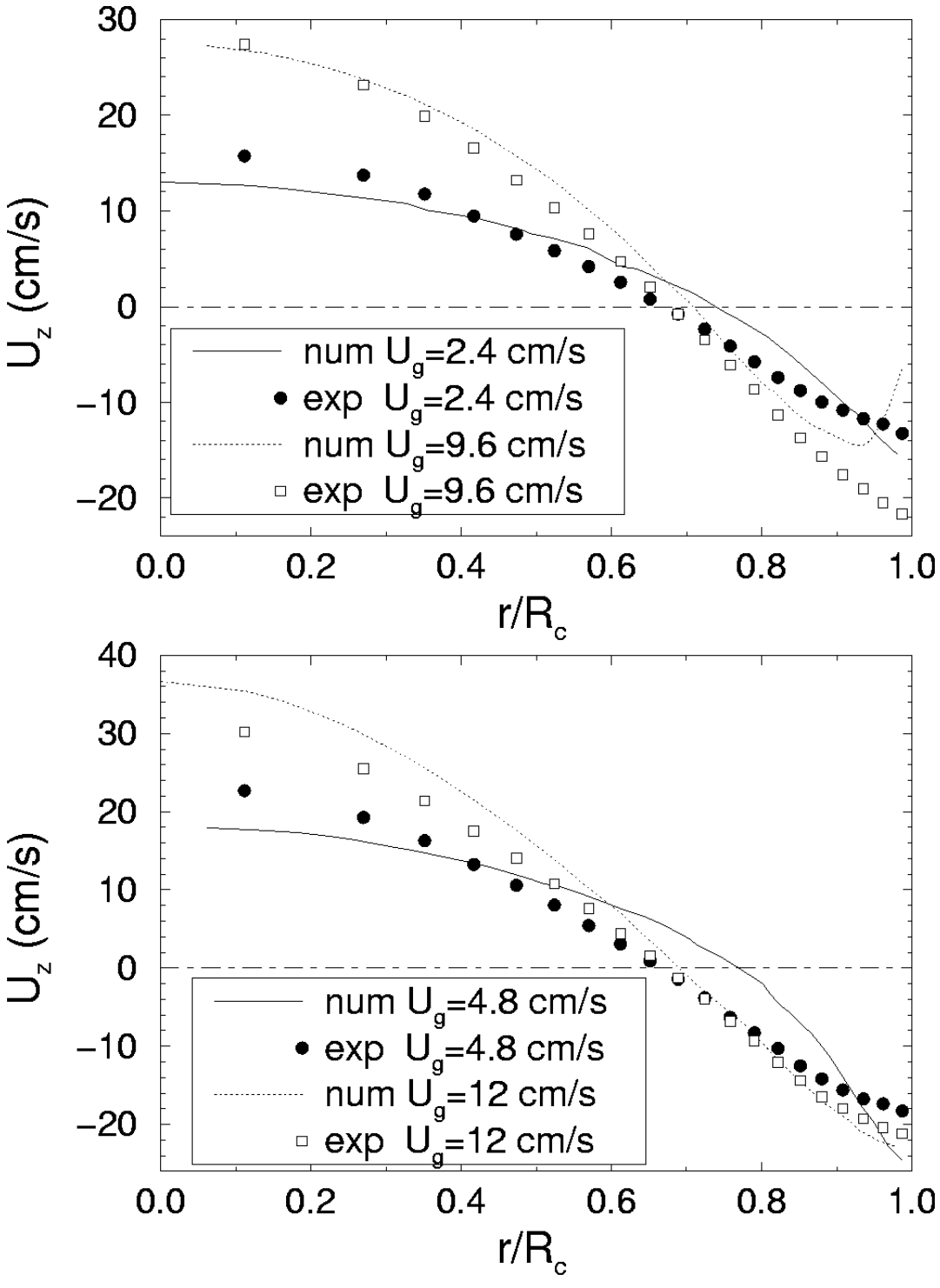

Figure 2.1 Comparison of Radial Profiles of Axial Liquid Velocity obtained from Simulation with Experimental Data measured by the CARPT Technique for a 14-cm Diameter Column

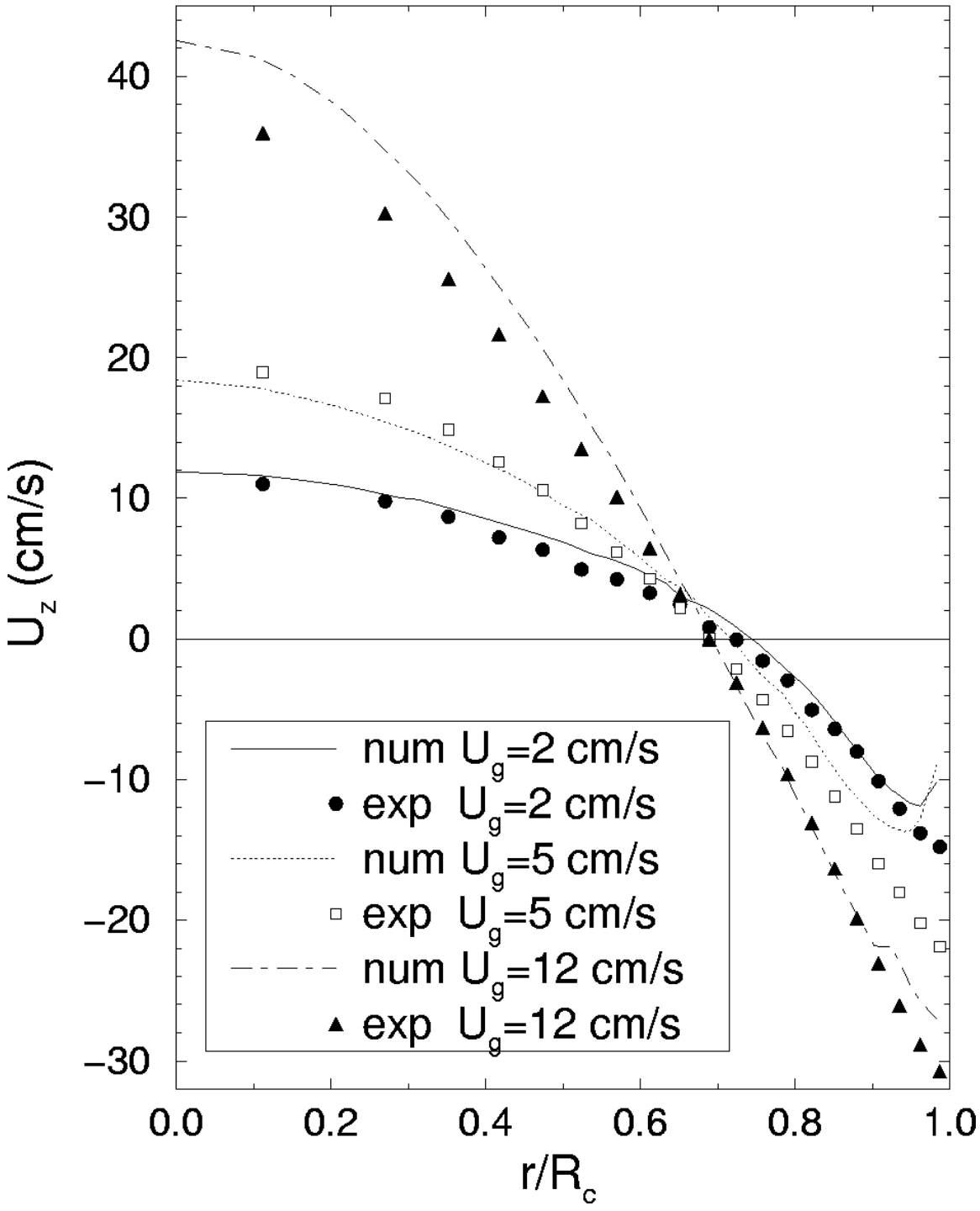

Figure 2.2 Comparison of Radial Profiles of Axial Liquid Velocity obtained from Simulation with Experimental Data measured by the CARPT Technique for a 19-cm Diameter Column

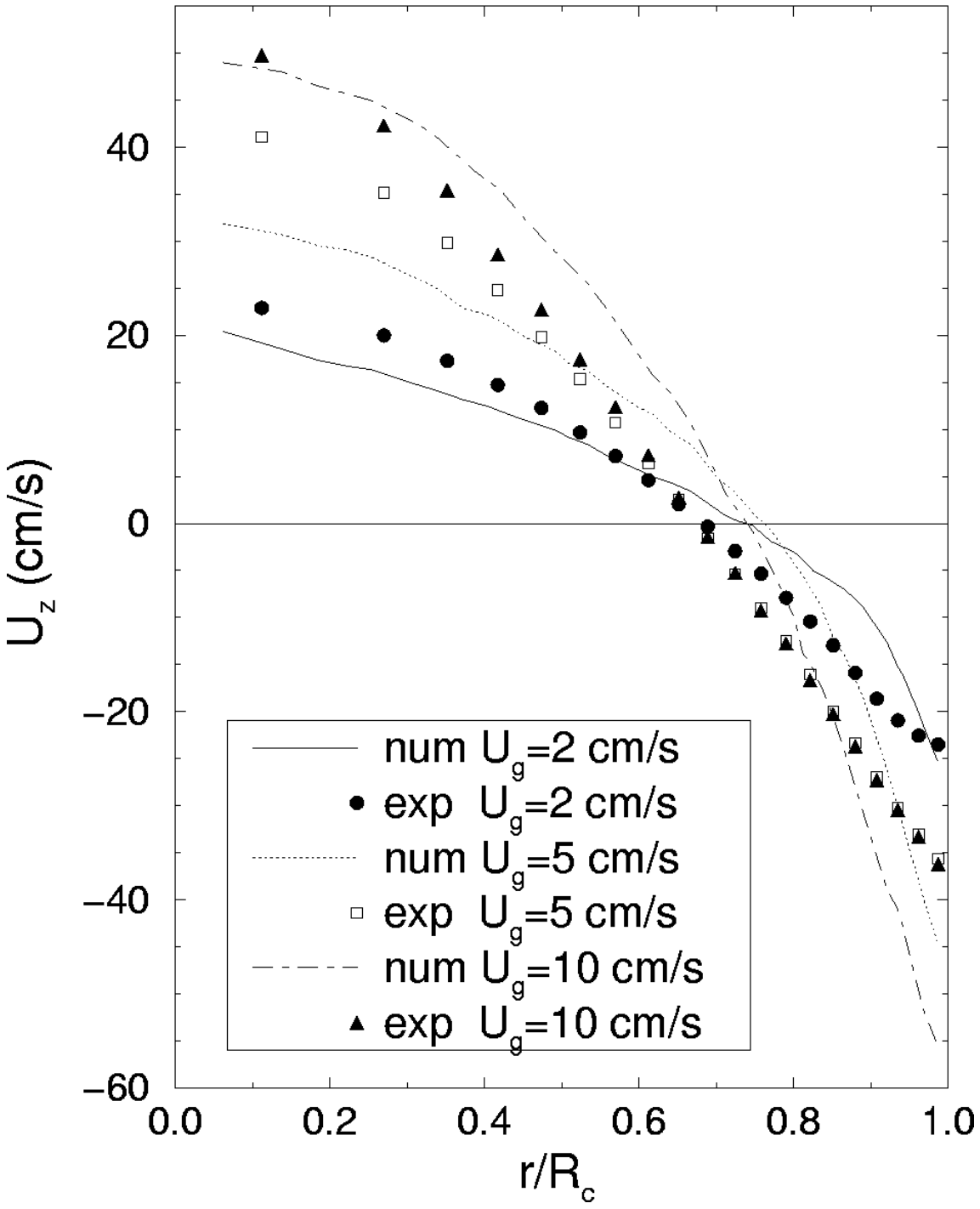

Figure 2.3 Comparison of Radial Profiles of Axial Liquid Velocity obtained from Simulation with Experimental Data measured by the CARPT Technique for a 44-cm Diameter Column

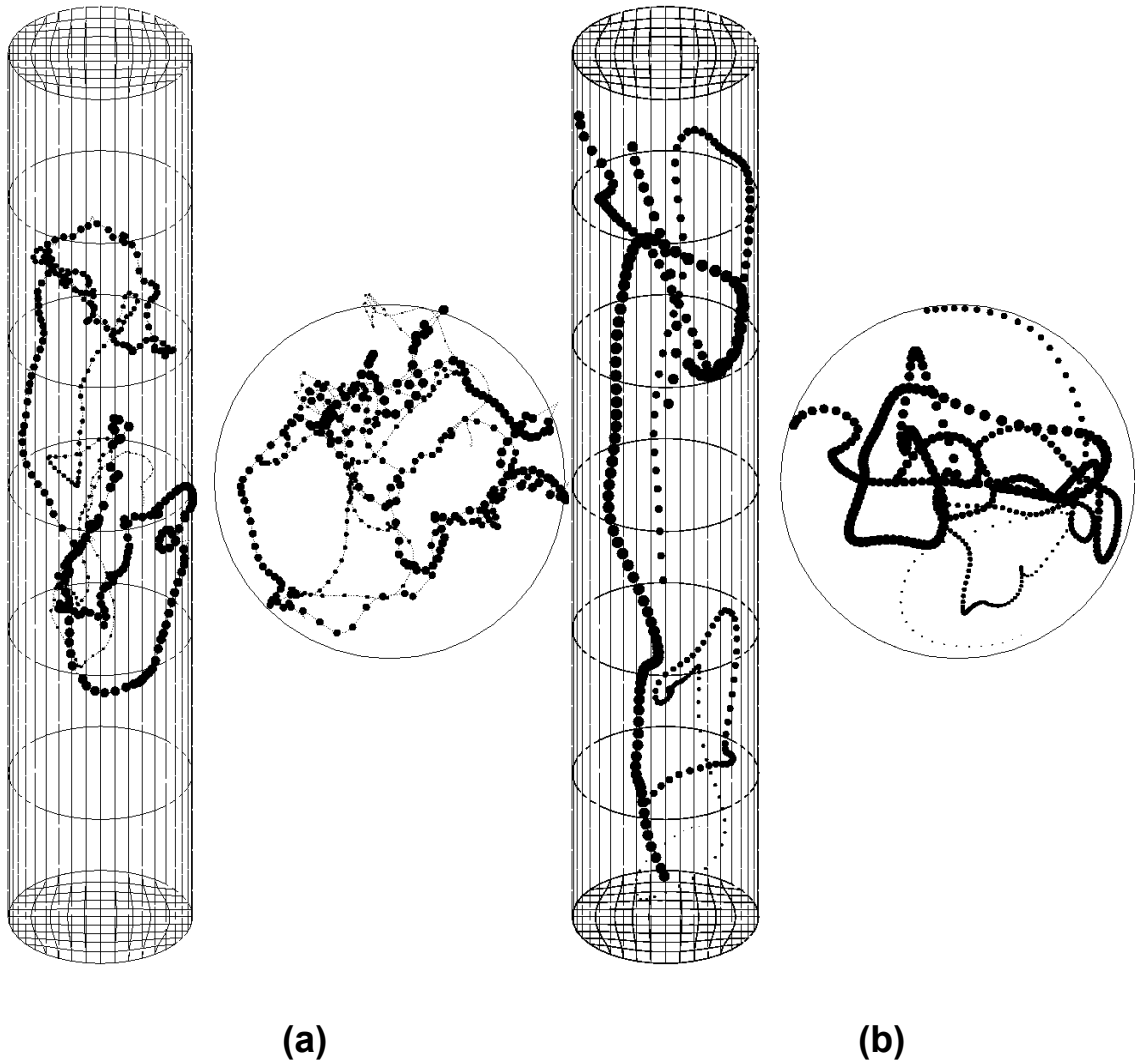

Figure 3.1 The Trajectory of the Tracer Particle in a 44-cm Diameter Column at U_g=10 cm/s: (a) CARPT experiment; (b) numerical particle tracking

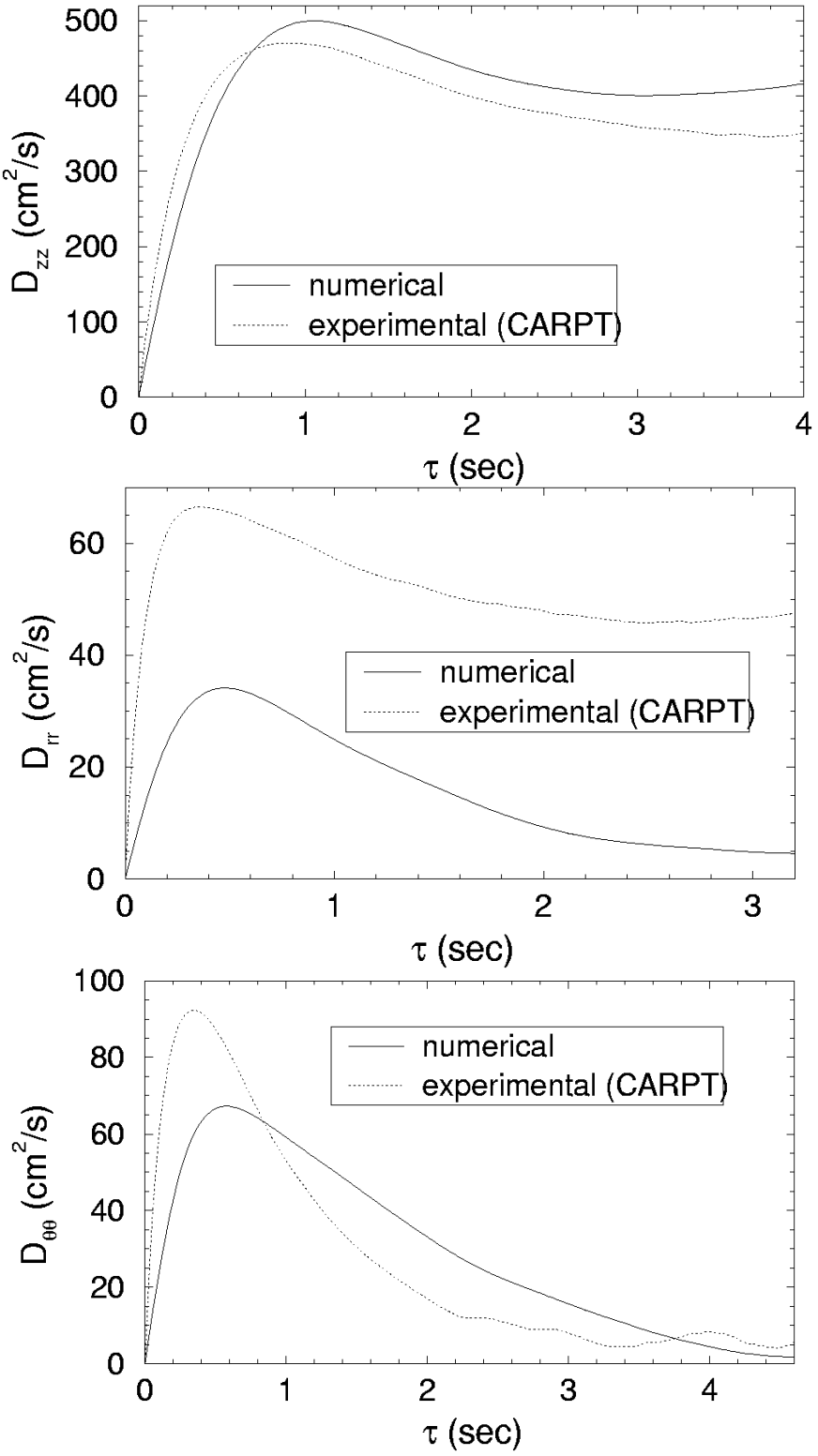

Figure 3.2 The Lagrangian Turbulent Diffusivities in the Middle Section of the 44-cm Diameter Column operated at a Superficial Gas Velocity of U_g=10 cm/s

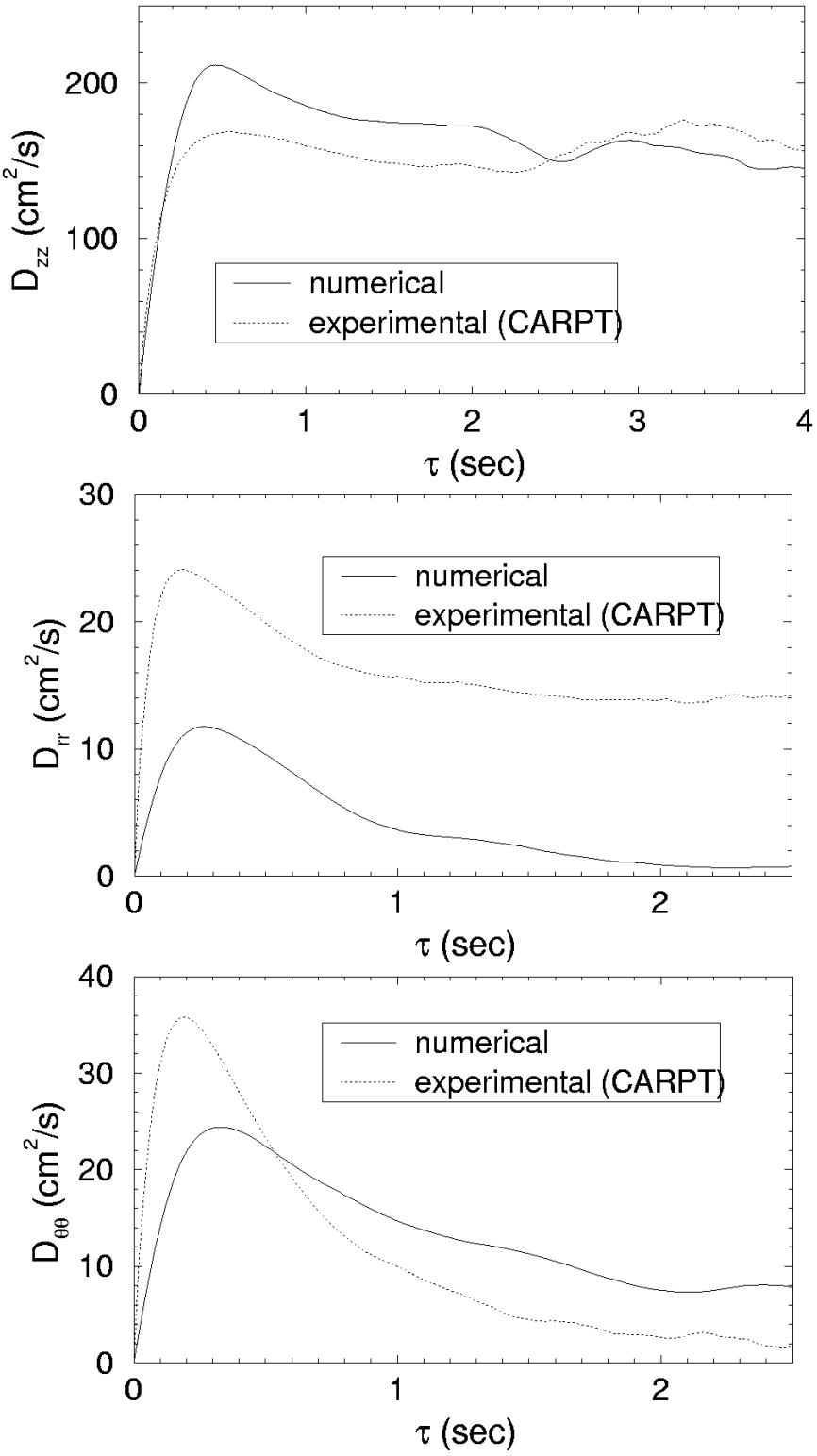

Figure 3.3 The Lagrangian Turbulent Diffusivities in the Middle Section of the 19-cm Diameter Column operated at a Superficial Gas Velocity of U_g=12 cm/s

THE OHIO STATE UNIVERSITY

The report for Ohio State for the period follows:

INTRINSIC FLOW BEHAVIOR IN A SLURRY BUBBLE COLUMN UNDER HIGH PRESSURE AND HIGH TEMPERATURE CONDITIONS

Quarter Report

(**Reporting Period:** January 1 to March 31, 2001)

Highlights

- The axial dispersion coefficients of the liquid phase were measured by the steady-state thermal dispersion method. It was found that the axial temperature distribution in terms of $\ln[(T-T_0)/(T_m-T_0)]$ is almost linear at various gas velocities.

- The axial dispersion coefficient increases significantly with increasing gas velocity. The effect of liquid velocity on the axial liquid mixing is small compared to the effect of gas velocity.

- The study of flow fields and Reynolds stresses at high pressures using a two-dimensional laser Doppler velocimetry (LDV) system was initiated. The LDV system was calibrated under ambient conditions.

- The axial liquid velocity profiles at different gas velocities under ambient conditions for the air-water system were measured using the LDV technique. The regime transition was identified based on the liquid velocity measurement, and the transition superficial gas velocity obtained was about 4 - 6 cm/s in the air-water system.

Work Conducted

1. Study of Axial Liquid-Phase Mixing in High-Pressure Bubble Columns

Experimental Setup

The experiments were conducted in a high-pressure column that was 5.08 cm I.D. and 1.0 m in height, including plenum, test and disengagement sections. Three pairs of quartz windows installed on the front and rear sides of each column provide direct visualization of flow behavior inside the column. The columns can be operated up to 22 MPa and 250^{o}C. The details of the high-pressure column are given in Luo et al. (1997).

The axial dispersion coefficients of the liquid phase were measured by the steady-state thermal dispersion method, i.e., introducing heat close to the outlet of the liquid phase and measuring the upstream temperature profile in the liquid. A cartridge heater with an outer diameter of 1.27 cm and a length of 5 cm was used as a source of heat. The maximum heating power was about 370W, and the heater was placed in the center of the column near the gas-liquid outlet. The axial temperature profile within the column was measured by copper-constantan thermocouples placed in the column center at different longitudinal positions, after the steady temperature distribution was attained. The inlet temperatures of liquid and gas were kept constant during the measurement. The maximum temperature difference across the column was controlled within several degrees celsius. A differential pressure transducer was installed to measure the overall gas holdup in the column simultaneously with the temperature measurement, which was required for calculating the axial dispersion coefficient. A perforated plate with 37 square pitched holes of 2.4 mm diameter was used as the distributor. The schematic of the experimental setup is shown in Figure 1.

In this study, nitrogen was used as the gas phase, and water and Paratherm NF® heat transfer fluid were used as the liquid phase. The physical properties of Paratherm NF® heat transfer fluid (μ_l=0.028 Pa·s, ρ_l=870 kg/m^3, σ=0.029 N/m at 27^{0}C and 0.1MPa) vary with pressure and temperature. Its physical properties at different pressures and temperatures are given in Yang et al. (2000). The liquid is in continuous operation and the liquid velocity varies up to 1.0 cm/s. The gas velocity varies up to 20 cm/s, which covers both the homogenous bubbling regime and heterogeneous bubbling regime.

Temperature Distribution

The measured axial temperature profiles in the column for air-water systems under ambient conditions are shown in Figure 2. It can be seen that the relationships between $ln[(T-T_0)/(T_m-T_0)]$ and z are almost linear at various gas velocities, which indicates that the model assumptions are reasonable. As the superficial gas velocity increases, the axial temperature profile becomes flat, which indicates the increased extent of liquid backmixing at higher gas velocities. The axial dispersion coefficient can be calculated based on the slope of temperature distribution curves and the gas holdup.

Comparison with Literature Data

To verify the validity of the measuring technique, the liquid mixing measurement was first conducted in the air-water system under ambient conditions, and the measured axial dispersion coefficients were compared with the literature data. The effects of gas and liquid velocities on the liquid mixing in the air-water system are shown in Figure 3. It was found that the axial dispersion coefficient increased significantly with increasing gas velocity. Generally, the axial liquid mixing in the nearly uniform dispersed bubbling regime was limited, and the axial dispersion coefficient was small. When the gas velocity was increased, the flow was in the coalesced bubbling or slugging regime, and the non-uniform flow behavior created significant axial liquid mixing. It was also found that the effect of liquid velocity on the axial liquid mixing was small compared to the effect of gas velocity. The axial dispersion coefficient in the air-water system slightly increased with an increase in liquid velocity, especially at low gas velocities. The

measured results were also compared to the available literature data obtained by various methods. Since liquid mixing strongly depends on column size, for comparison purposes, the literature data obtained in different column sizes were converted into the column size used in this study (i.e., 5.08 cm) by using the relationship between the axial dispersion coefficient and the column diameter observed in their studies. If such a relationship was not available in some of the literature studies, the effect of diameter was accounted for by using the following relationship:

$$E_l \propto D^{1.4}. \qquad (1)$$

Many studies have proven this relationship capable of predicting the effect of scaleup on liquid mixing (Deckwer et al., 1974; Wendt et al., 1984). The comparison shows that the experimental data obtained in this study using the thermal dispersion technique agree well with most literature data, which further verifies the validity of the measuring technique. It was also found that the data converted from large columns (e.g., >10cm) (Deckwer et al., 1974; Wilkinson et al., 1993) are lower than the experimental data obtained in small columns (Kato and Nishiwaki, 1972; Wendt et al., 1984). This is possibly due to the different mixing behavior between small and large columns. The detailed information from various literature studies used in the figure is provided in Table 1.

2. Study of Flow Fields and Reynolds Stresses

LDV System Setup

To measure the velocity profiles of the liquid phase, a two-dimensional laser Doppler velocimetry system in the backscatter mode was used. Figure 4 shows the schematic of the LDV system. The laser Doppler velocimetry system includes a 300-mW, air-cooled, argon-ion laser system and a beam separator. Two pairs of laser beams with the known wavelengths of 514.5 and 480 nm are generated. The light is transmitted through a fiber optic cable and a probe with 25-cm focal-length lens. This configuration yields 48 fringes with fringe spaces of 3.40 and 3.22 μm and measurement volumes of 0.164×0.164×2.162 mm and 0.156×0.156×2.05 mm for the 514.5- and 480-nm wavelengths, respectively. The scattered light is collected through the same probe (i.e., backscatter mode) and a detector, and processed by a signal processor.

To measure the turbulent velocities of the liquid phase, neutrally buoyant Pliolite particles, 1.02 g/cm^3 in density with a size range of 20 - 50 μm, are used as the liquid seeding particles because these kinds of particles are able to follow the liquid flow, even in turbulent conditions. The distortion of laser beams is avoided, since the flat quartz windows installed in the high-pressure cylindrical column are used for the penetration of laser beams.

The application of the LDV technique in bubbly flows is not as trivial as in single-phase flows because of the existence of a dispersed phase. One of the most challenging issues regarding the application of the LDV technique in bubbly flows is proper discrimination among different phases. To reduce the effect of bubbles, the LDV system is operated in

the backscatter mode because the signals obtained in the backscatter mode predominantly represent the liquid phase (Mudde et al., 1998).

All measurements in this study were sampled between 600 and 1200 seconds, and under such a sampling time range, the reliability of the measurement was excellent. The data rate ranged from 10 to 100 Hz. The sampling rate was relatively low because of the system limitation, for example, the low power source of the laser system and relative thickness of the quartz windows. The sampling rate strongly depended on the distance between the measurement point and the wall due to the light scattering caused by bubbles. Ohba et al. (1976) showed that the exponential relationship of the intensity of the scattered light, I, with the penetration depth of the laser beams, l, and the gas holdup, ε_g, is

$$\frac{I}{I_0} = \exp\left(-\frac{3}{2}\frac{l}{d_b}\varepsilon_g \right), \tag{2}$$

where I_0 is the light intensity without bubbles and d_b is the distance occupied by a bubble in the direction parallel to the laser beam.

By using one pair of laser beams, the complete radial profile of axial liquid velocity can be obtained, which is referred to as the 1D measurement mode in this study. On the other hand, only half profiles of axial and tangential velocities can be measured using two pairs of laser beams (i.e., 2D measurement mode), because the quartz windows used are not wide enough to allow all the laser beams to pass through.

LDV measurements are currently conducted in the 2-inch, high-pressure column and will also be carried out in the 4-inch vessel. Three pairs of flat quartz windows have been installed on the front and rear sides of the column, and each window is 1.27cm in width and 9.3cm in height. Water is currently used as the liquid phase, and the system is operated in the batch mode. Paratherm NF® heat transfer fluid will also be used to study the effect of liquid properties. Figure 5 is the schematic diagram of the experimental setup of the LDV system in the high-pressure bubble column. The effects of operating conditions and design variables, such as pressure, temperature, gas velocity, axial position, column dimension, liquid properties, and internals will be investigated systematically.

LDV System Calibration and Test

Figure 6 shows the experimental results of liquid velocities obtained from both the 1D and 2D measurement modes under ambient conditions. It was found that the flow structure in bubble columns is axisymmetric. The repeatability of measurements is also shown in Figure 6, and the results are reproducible.

Figure 7 compares LDV measurements with literature data reported by Chen et al. (1999). It was found that the results from LDV measurements agree well with those obtained using different measurement techniques.

Effect of Gas Velocity

Figure 8 shows liquid axial velocity profiles measured under ambient conditions at different gas velocities. The liquid axial velocity increases with increasing superficial gas velocity in the central region of the bubble column. The velocity profile becomes steeper at higher gas velocities. There is gross liquid circulation in the column, and the reverse of liquid flow occurs at the point where r/R = 0.7, which matches other literature studies.

Transition of Flow Regime

Figure 9 shows the effect of gas velocity on axial liquid velocity at the column center. The axial liquid velocity at the center point increases with an increase in the superficial gas velocity; however, the increase in rate varies with gas velocity. At low gas velocities, the center liquid velocity increases quickly with increasing gas velocity. When the gas velocity exceeds a certain value (i.e., about 4.8 cm/s in this study), the increase in rate of center liquid velocity with gas velocity becomes smaller. The point that the increase in rate suddenly changes can be defined as the flow regime transition point.

In order to further verify the transition point identified based on the liquid velocity measurement, gas holdup was also measured using a pressure transducer, and the drift-flux method was used to identify the regime transition.

Figure 10 shows the gas holdup data in the 2-inch column under ambient conditions, and Figure 11 shows the relationship between the drift-flux and the gas holdup. The transition velocity obtained based on the drift-flux method is about 5.8 cm/s, as shown in Figure 10, which agrees with the results obtained from our LDV measurements and the findings in most literature studies, in the range of 4.0 to 6.0 cm/s (Yamashita and Inoue, 1975; Drahos et al., 1992; Hyndman and Guy, 1995; Bakshi et al., 1995).

Future Work

Ohio State's future work will involve the measurement of the axial dispersion coefficients of the liquid phase in bubble columns by the steady-state thermal dispersion method. Work will also be done on quantification of the axial liquid velocity profiles and Reynolds normal and shear stresses.

Notations

E_l liquid-phase dispersion coefficient, m^2/s
T temperature at axial position z, ^0C
T_0 liquid inlet temperature, ^0C
T_m liquid outlet temperature, ^0C
U_l superficial liquid velocity, m/s
z axial height from the gas-liquid outlet, m
ε_g gas holdup, dimensionless

References

Aoyama, Y., K. Ogushi, K. Koide, and H. Kubota, "Liquid mixing in concurrent bubble columns," *J. Chem. Eng. Japan*, **1**, 158 (1968).

Bakshi, B. R., H. Zhong, P. Jiang, and L.-S. Fan, "Analysis of flow in gas-liquid bubble columns using multi-resolution methods," *Chem. Eng. Res. Des.*, **73**, 608 (1995).

Chen, J., A. Kemoun, M. H. Al-Dahhan, M. P.Dudukovic, D. J. Lee, and L.S. Fan, "Comparative hydrodynamics study in a bubble column using computer-automated radioactive particle tracking (CARPT)/computed tomography (CT) and particle image velocimetry (PIV)," *Chem. Eng. Sci*., **54**, 2199 (1999).

Deckwer, W. D., R. Burckhart, and G. Zoll, "Mixing and mass transfer in tall bubble columns," *Chem. Eng. Sci.*, **29**, 2177 (1974).

Drahos, J., J. Zahradnik, M. Fialova, and F. Bradka, "Identification and modelling of liquid flow structures in bubble column reactors," *Chem. Eng. Sci.*, **47**, 3313 (1992).

Holcombe, N. T., D. S. Smith, H. N. Knickle, and W. O'Dowd, "Thermal dispersion and heat transfer in nonisothermal bubble columns," *Chem. Eng. Commun.*, 21, 135 (1983).

Hyndman, C. L., and C. Guy, "Gas phase hydrodynamics in bubble columns," *Chem. Eng. Res. Des.*, **73**, 302 (1995).

Kato, Y. and A. Nishiwaki, "Longitudinal dispersion coefficient of a liquid in a bubble column," *Int. Chem. Eng.*, **12**, 182 (1972).

Mudde, R. F., J. S. Groen, and H. E. A. Van Den Akker, "Application of LDA to bubbly flows," *Nuclear Engi. And Design*, **184**, 329 (1998).

Ohba, K., I. Kishimoto, and M. Ogasawara, "Simultaneous measurement of local liquid velocity and void fraction in bubbly flows using a gas laser – Part I: Principle and measuring procedure," *Tech. Rep. Osaka Univ*., **26**, 547 (1976).

Wendt, R., A. Steiff, and P. M. Weinspach, "Liquid phase dispersion in bubble columns," *Ger. Chem. Eng.*, **7**, 267 (1984).

Yamashita, F., and H. Inoue, "Gas hold-up in bubble columns," *J. Chem. Eng. Japan*, **8**, 334 (1975).

Table 1 Relevant Information from Various References used in Figure 3 regarding Liquid Mixing in an Air-Water System under Ambient Conditions

Reference	Technique	U_g (cm/s)	U_l(cm/s)	D (cm)	U_l effect	Relation between E_l and D
Aoyama et al. (1968)	mass & thermal	0.3~8	0.18~0.62	5.0	No	$D^{1.5}$
Kato & Nishiwaki (1972)	mass	1~25	0.7~1.3	6.6	No	N/A
Deckwer et al. (1974)	mass	1~15	0.71	20	N/A	$D^{1.4}$
Hikita & Kikukawa (1974)	mass	4.3~33.8	0	10	N/A	$D^{1.25}$
Mangartz & Pilhofer (1981)	thermal	0.5~18	0~6	10	No	$D^{1.5}$
Holcombe et al. (1983)	thermal	0~60	0~2	7.8	N/A	$D^{1.33}$
Wendt et al. (1984)	mass & thermal	1.5~30	0.2~4.5	6.3	No	$D^{1.4}$
Wilkinson et al. (1993)	Mass	2~20	0	15.8	N/A	N/A
This work	Thermal	2~20	0.34~1.0	5.08	Small	N/A

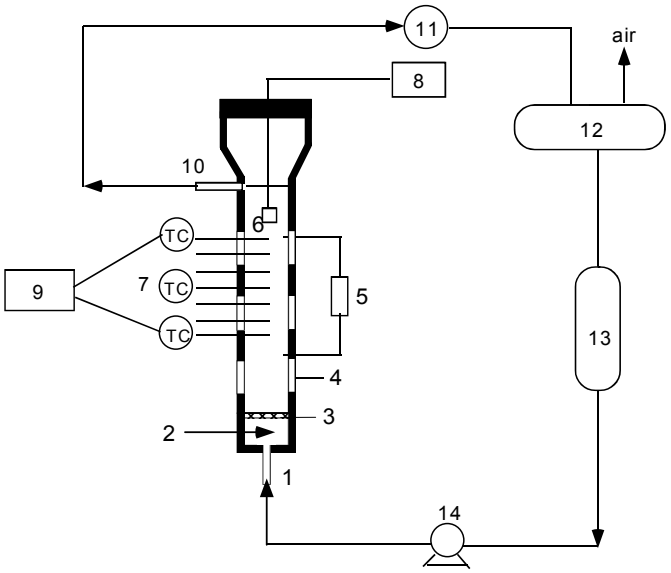

1. Liquid inlet
2. Gas inlet
3. Perforated plate distributor
4. Quartz window
5. Pressure transducer
6. Heater
7. Thermocouples
8. DC power
9. Computer and data acquisition system
10. Gas and liquid outlet
11. Back pressure regulator
12. Gas/liquid separation tank
13. Liquid supply tank
14. Liquid pump

Figure 1 Schematic of Experimental Setup for the Measurement of Liquid-Phase Mixing

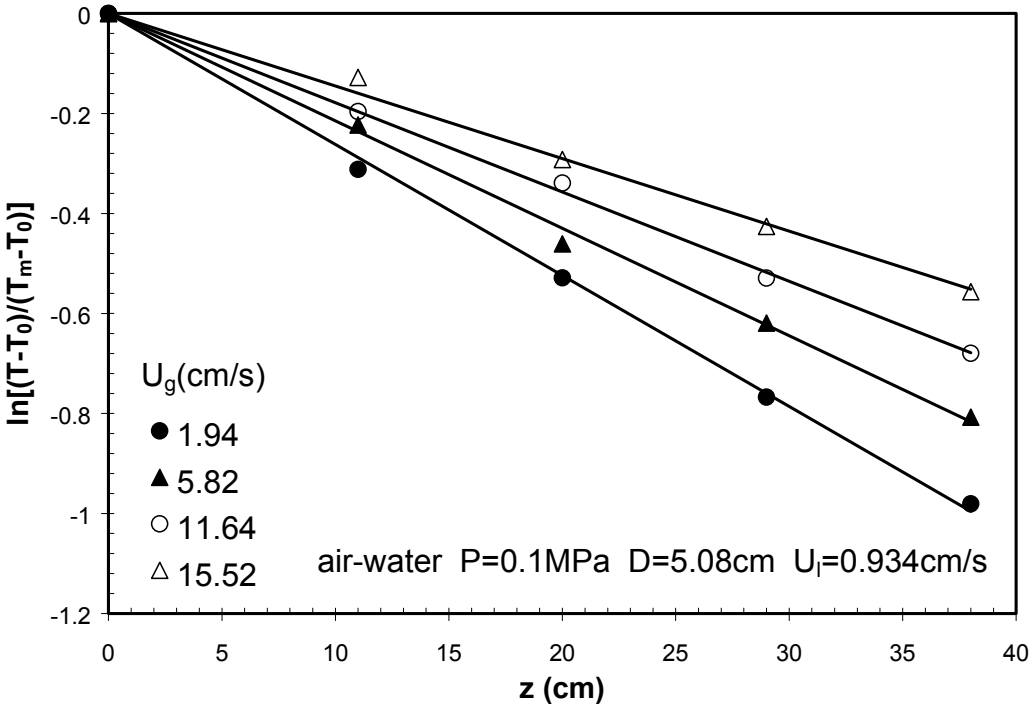

Figure 2 Typical Temperature Distribution Profiles in the 5.08 cm Column (Air-Water System)

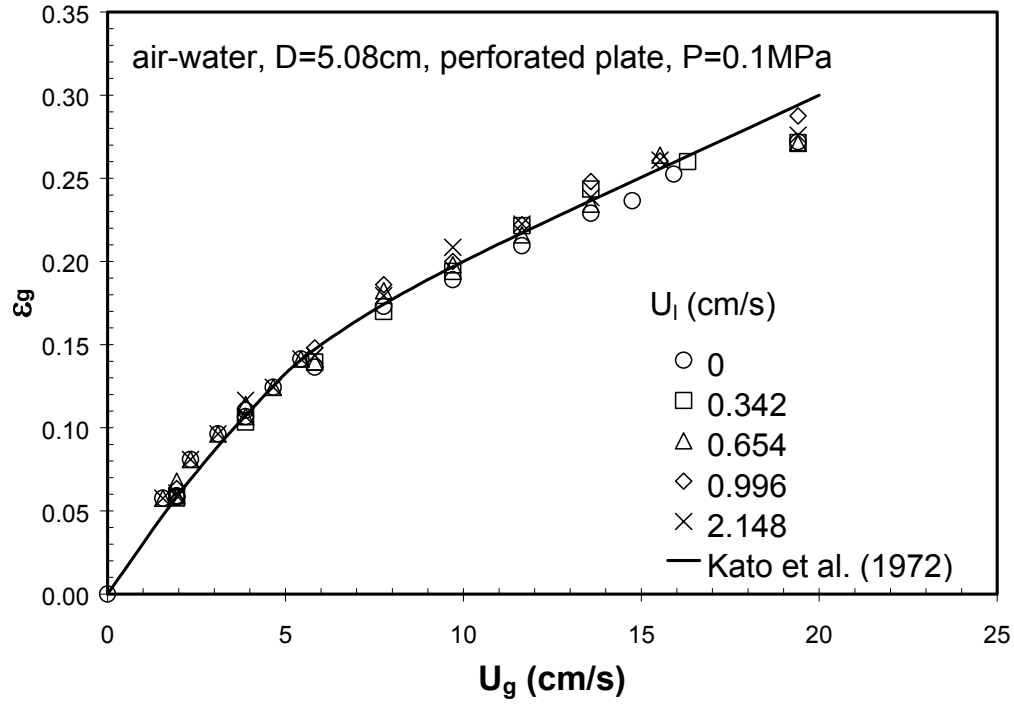

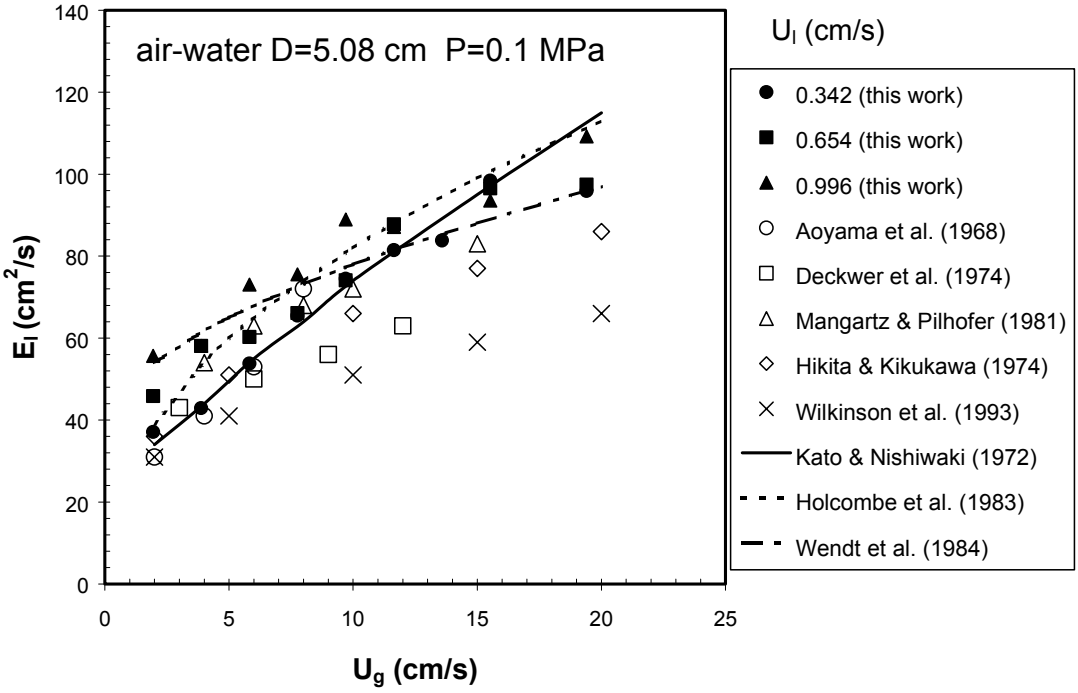

Figure 3 Comparison of Experimental Data with Available Literature Data for Air-Water Systems under Ambient Conditions

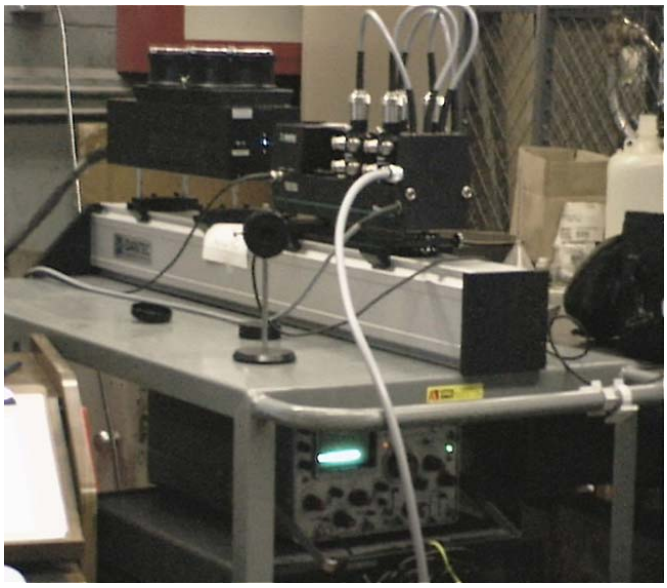

(a) LDV system used in this study

(b) Laser head and high-pressure bubble column

Figure 4 Schematic of LDV Measurement System

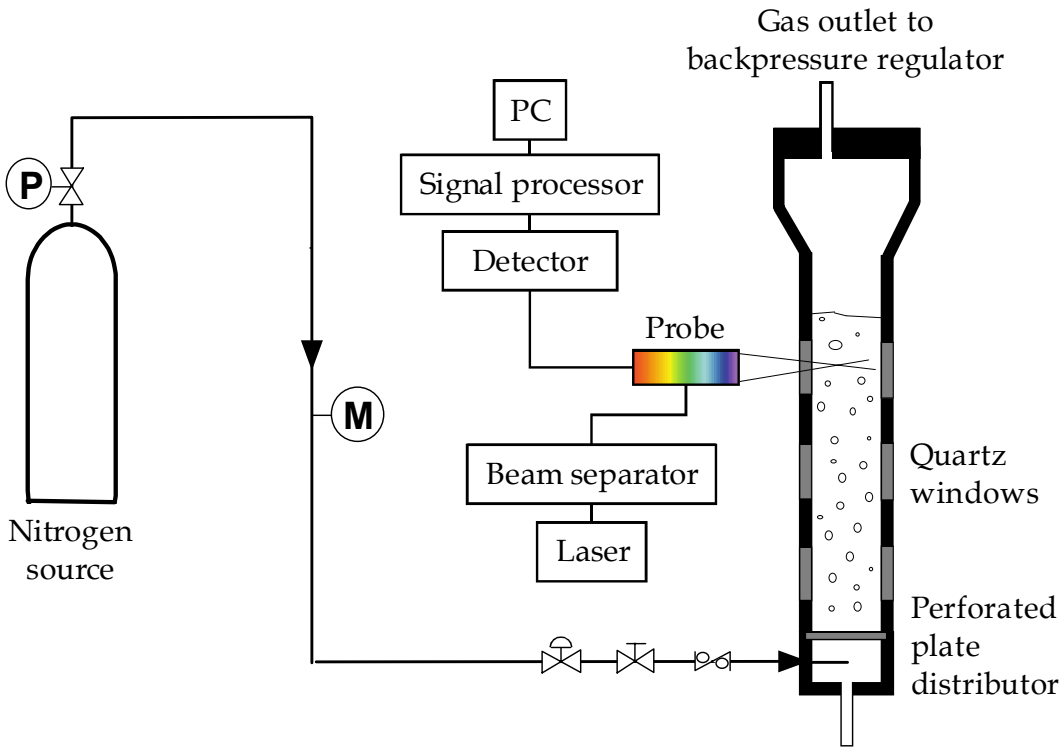

Figure 5 Schematic Diagram of LDV Measurement in the High-Pressure Vessel

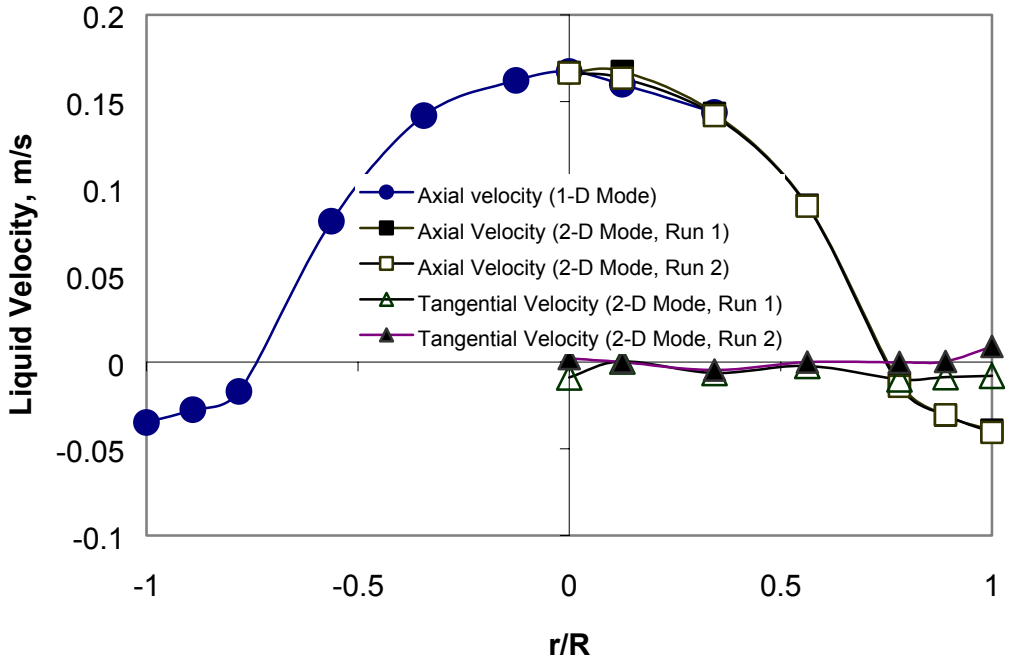

Figure 6 Comparison of Liquid Velocities measured by 1D and 2D Measurement Modes (P=0.1 MPa, D_c=5.1 cm, U_g=2.5 cm/s)

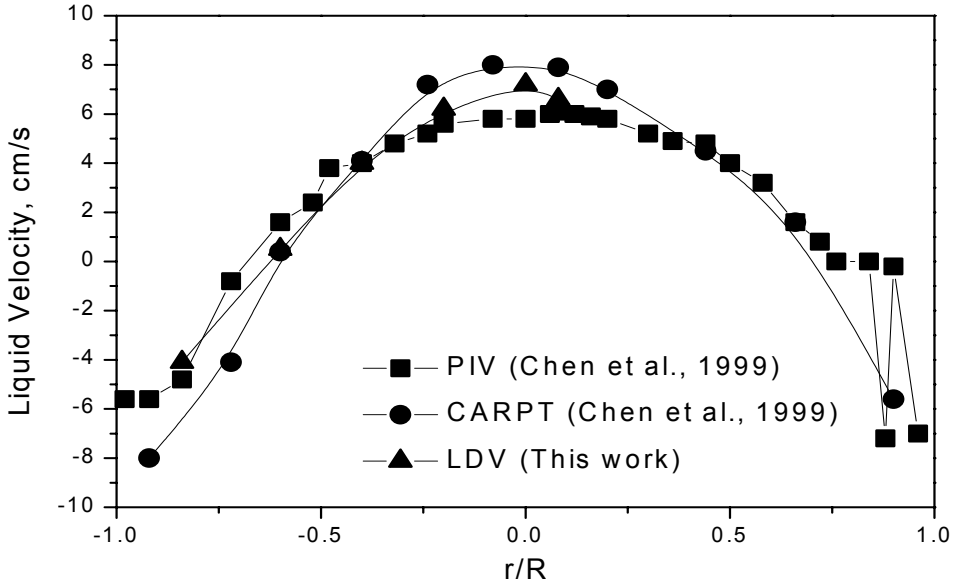

Figure 7 Comparison of LDV Measurement with Literature Data (P=0.1 MPa, U_g=1.9 cm/s)

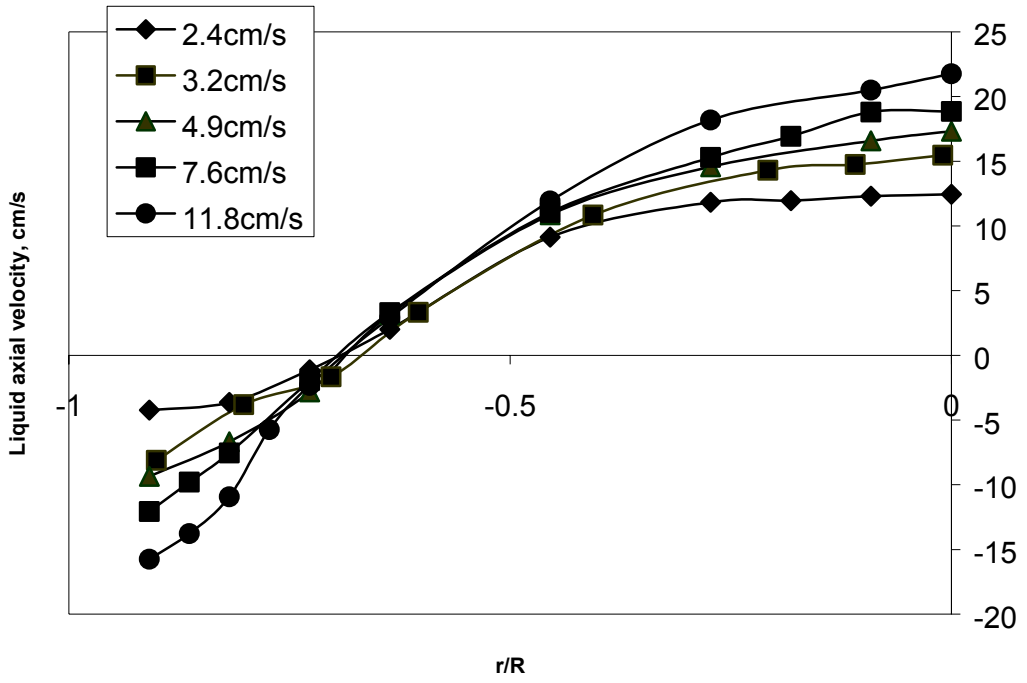

Figure 8 Axial Liquid Velocity Profiles under Ambient Conditions in the 2-inch Bubble Column

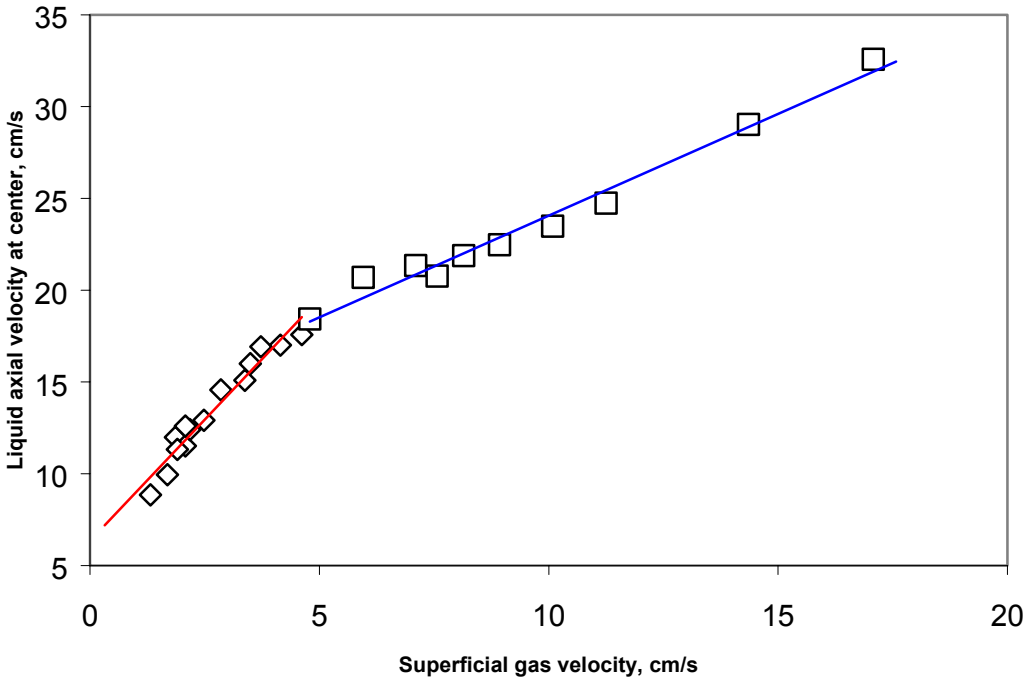

Figure 9 Effect of Gas Velocity on the Axial Liquid Velocity at Column Center

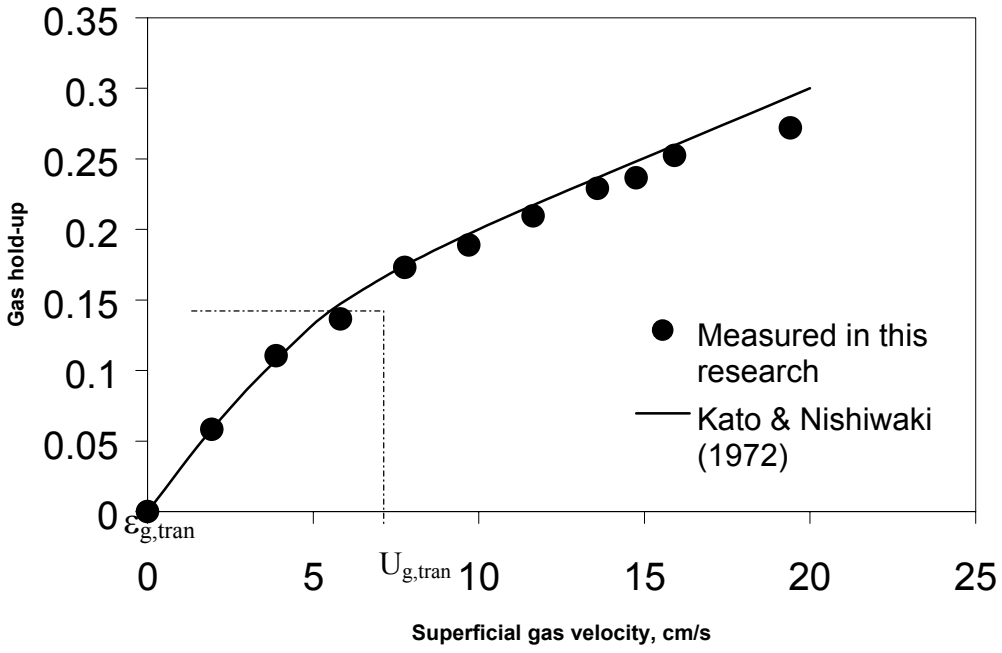

Figure 10 Effect of Superficial Gas Velocity on Gas Holdup in the 2-inch Bubble Column

($U_{g,tran}$ = 5.8 cm/s)

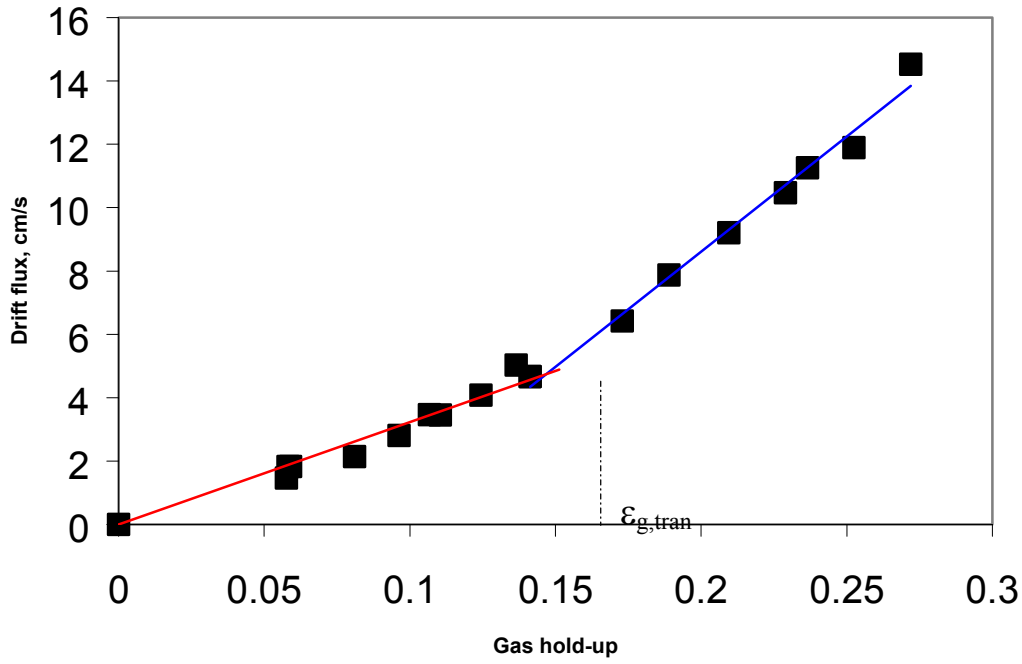

Figure 11 Identification of Flow Regime Transition based on the Drift-Flux Method ($\varepsilon_{g,tran} = 0.14$)

IOWA STATE UNIVERSITY

The report from Iowa State University for the period follows.

CFD INVESTIGATION OF SLURRY BUBBLE COLUMN HYDRODYNAMICS

Fifth Quarterly Report

Budget Year 2 – 5th Quarter
For
January 1 – March 31, 2001

Highlights

- Used CFDLIB to simulate conditions described in Zenit et al. (J. Fluid Mech., vol. 420, pp. 1-36, 2000) to validate simulation result.

- Determined that small column diameters cannot be accurately represented by periodic boundary conditions.

- Studied free-slip boundary conditions versus periodic boundary conditions to determine whether or not free-slip boundary conditions could be a suitable alternative.

3D Bubble Column Results

During this quarter, work at Iowa State University continued using the 3D version of CFDLIB to simulate flow within air-water bubble columns.

Jyoti Singh has used CFDLIB to simulate the column described in the paper by Zenit et al. (J. Fluid Mech., vol. 420, pp. 1-36, 2000). This experiment uses a column that is 2 m high, and bubbles are produced uniformly from a 2-cm by 20-cm capillary array at the bottom of the column. These dimensions allow one to assume nearly 2D flow within the center of the column. Consistent with the experimental measurements, bubbles are assumed to be almost spherical and 1-2 mm in diameter.

Simulations were first performed using a domain size equal to that described by Zenit et al. (J. Fluid Mech., vol. 420, pp. 1-36, 2000), with a grid spacing of (width) 1 cm by (height) 0.4 cm by (depth) 1 cm. Air was introduced uniformly at 2 cm/s. These CFDLIB simulations illustrated that air predominantly rises through the center of the column, as shown in Figure 1. This was in disagreement with the results described by Zenit et al. (2000), in which air is uniformly distributed within the column. Simulations resulted in an average air volume fraction of 7 percent at 25 seconds, a value lower than that found experimentally (10 percent). Figures 2-4 show the water velocity profiles at 25 seconds. Note that due to the small number of grid cells in the z direction (2), W1 shown in Figure 4 is not fully resolved.

In order to improve the resolution, another set of simulations was then performed under the same conditions. However, a smaller grid size was used, with 0.5-cm cells along the column height, 0.5 cm along the column width, and 0.25 cm along the column depth. These simulations resulted in an average air volume fraction of 10.15 percent after 10 seconds of simulation time. This value was much closer to the experimental value of 10 percent measured with an impedance probe, and 11 percent measured with a gas flow meter.

The results of the 3D “high-resolution” simulations are very encouraging. We will continue to collect simulation data at various air superficial velocities for comparison with experimental data. Our long-term goal will be to use these data to develop a multiphase turbulence model that is computationally more efficient than the “high-resolution” simulations.

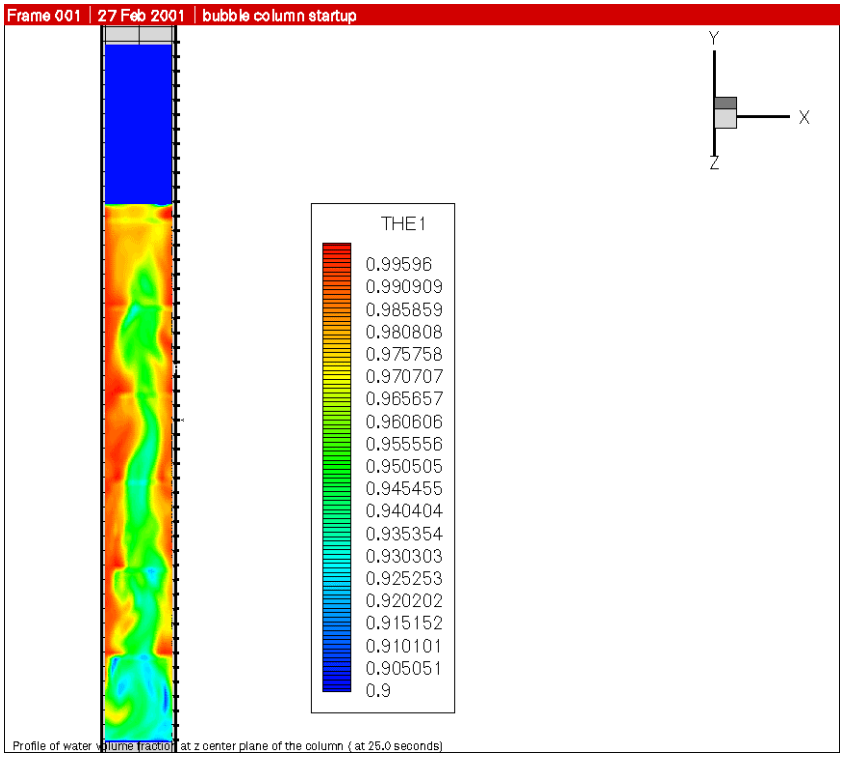

Figure 1 Profile of Water Volume Fraction at Z-Center Plane of the Column at 25 seconds (blue color represents values 0.0-0.9)

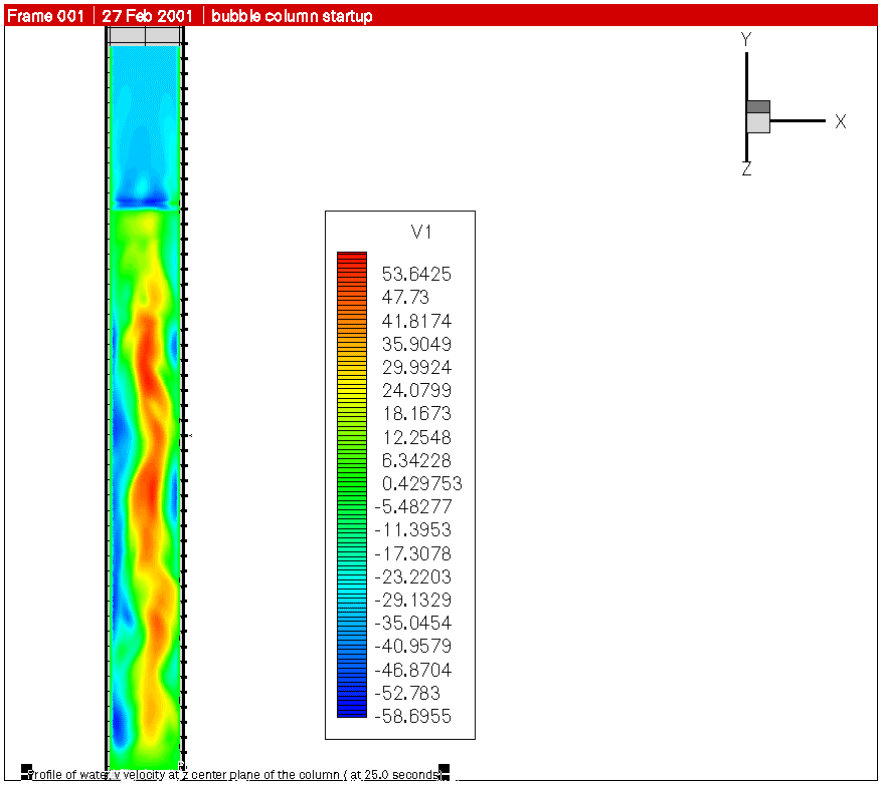

Figure 2 Profile of Water Velocity in the Y-Direction at the Z-Center Plane of the Column at 25 seconds

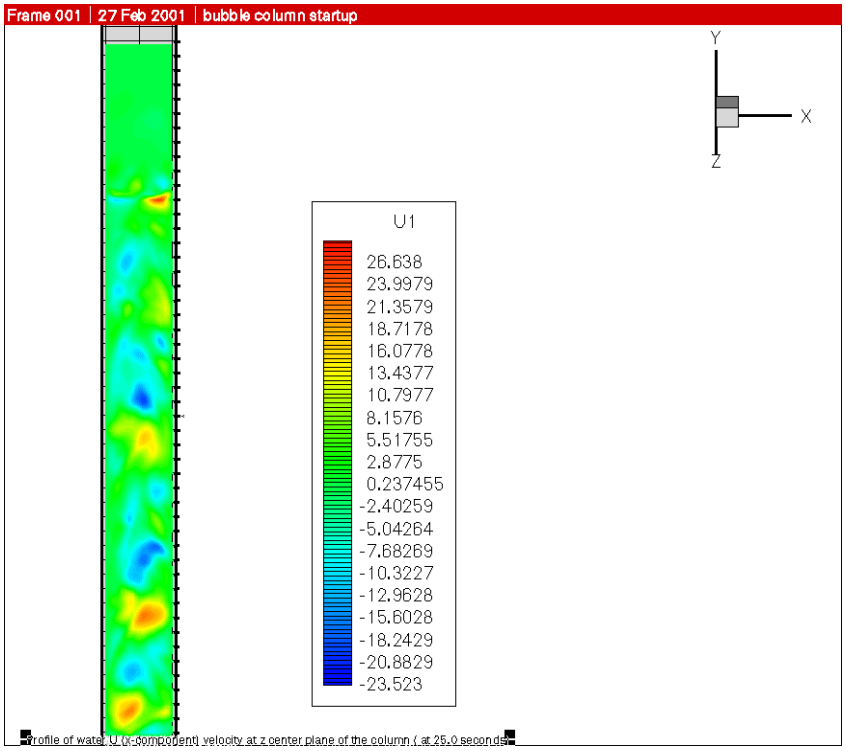

Figure 3 Profile of Water Velocity in the X-Direction at the Z-Center Plane of the Column at 25 seconds

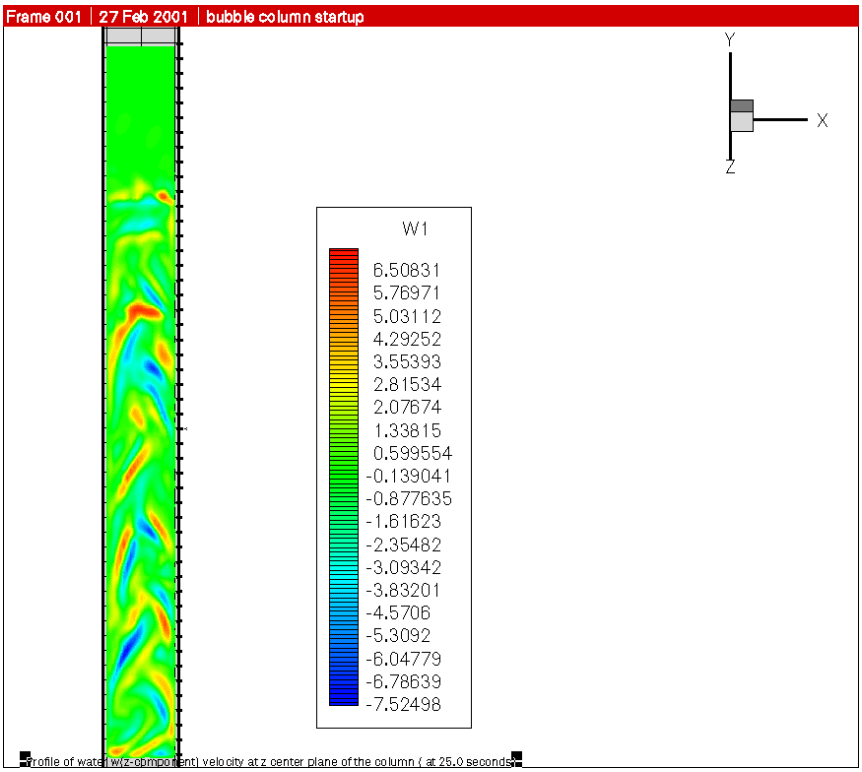

Figure 4 Profile of Water Velocity in the Z-Direction at the Z-Center Plane of the Column at 25 seconds

Effect of Boundary Conditions

Sarah Monahan has been using CFDLIB for 3D simulations utilizing periodic boundary conditions. The use of periodic boundary conditions allows one to neglect effects at the column walls. Simulations first used dimensions of 200 cm in height, 20 cm in width, and 2 cm in depth, the same dimensions used in the paper by Zenit et al. (J. Fluid Mech., vol. 420, pp. 1-36, 2000). Air bubbles were assumed to be spherical, with a diameter of 1.5 mm, and were introduced uniformly to the column at 2 cm/s. Cubic grids of both 1 and 0.5 cm were studied. The finer grid size generated a more detailed representation of the air volume fraction within the column. An example of this is illustrated in Figures 5 and 6.

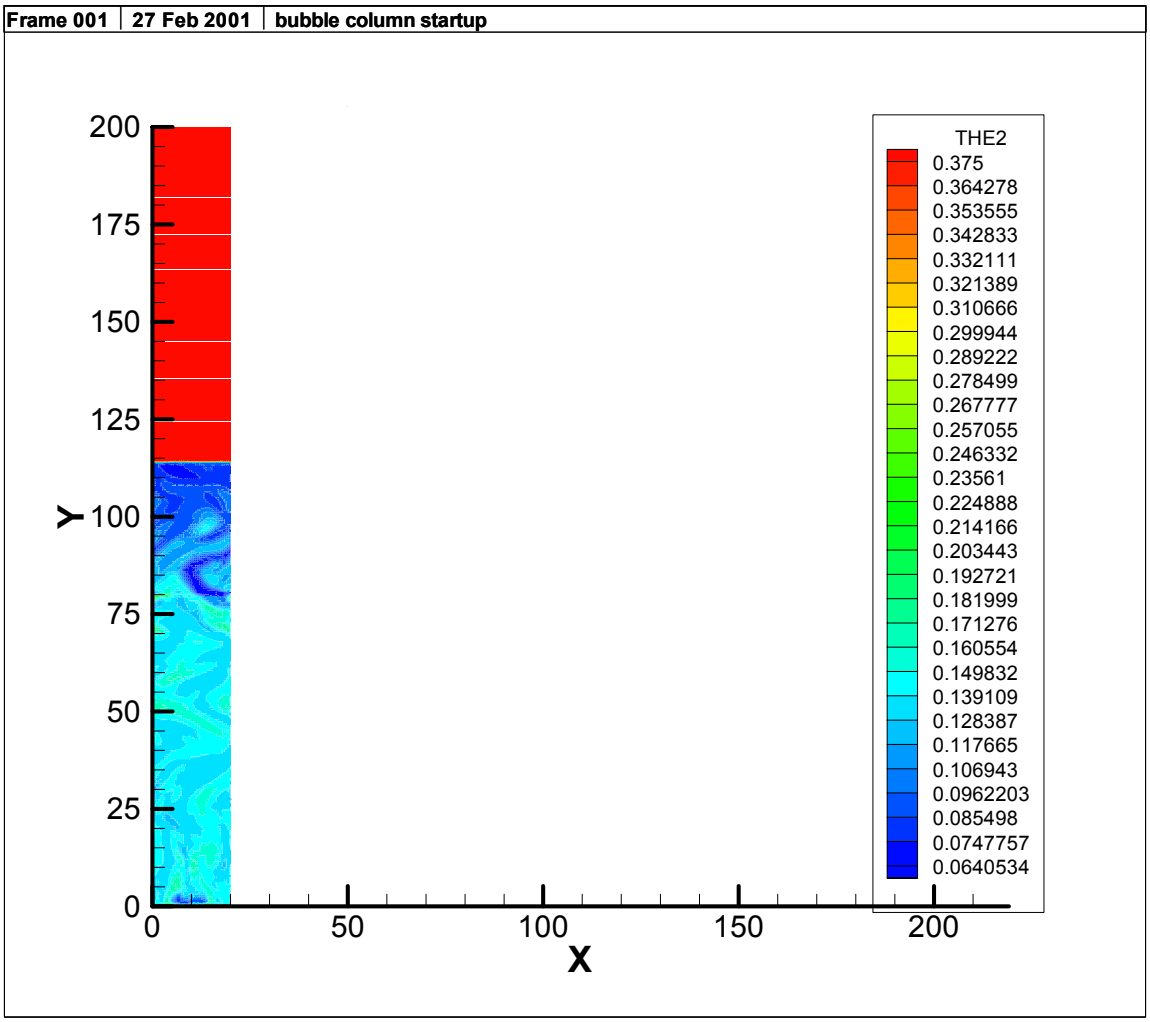

Figure 5 Volume Fraction of Air for the 0.5-cm Grid Simulation

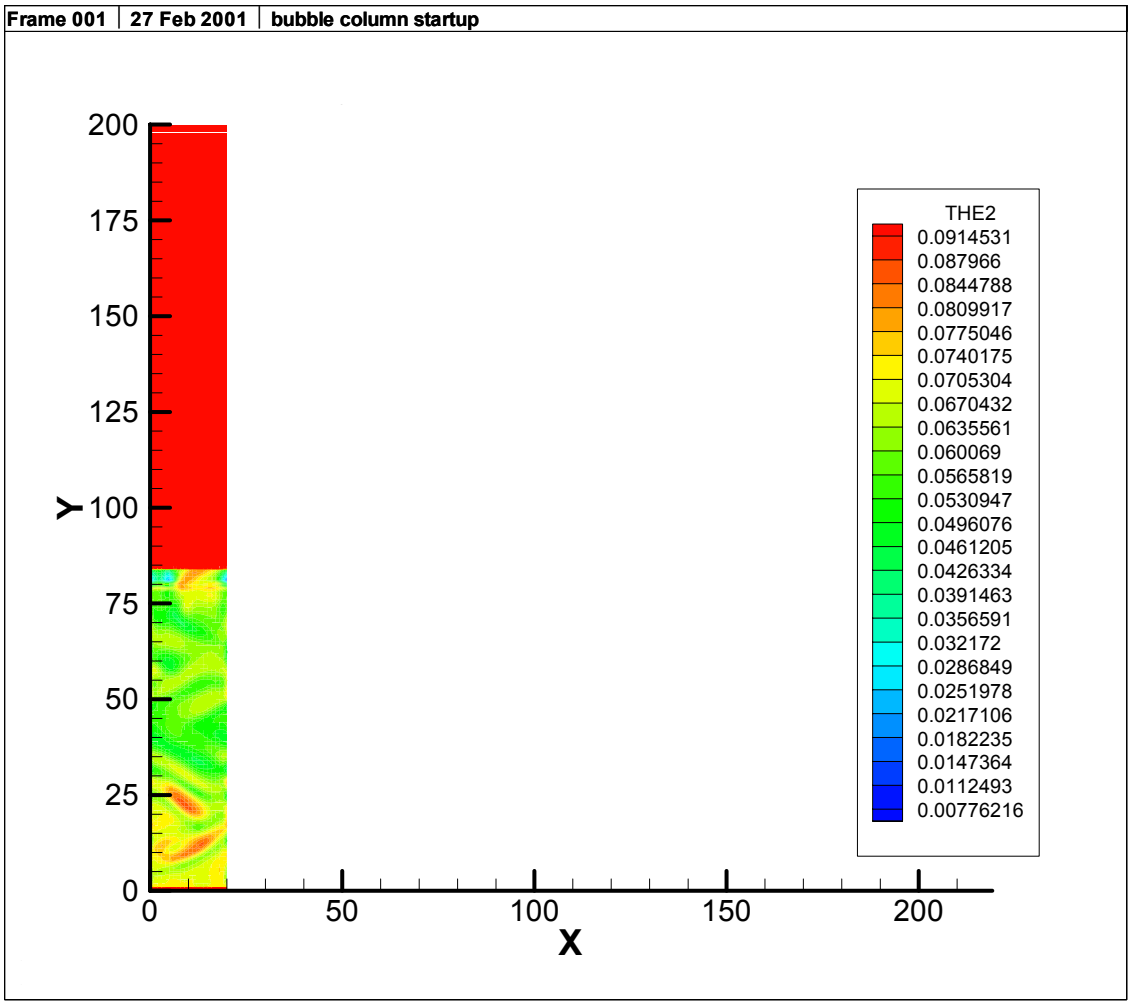

Figure 6 Volume Fraction of Air for the 1-cm Grid Simulation

With a 20-cm wide column and periodic boundary conditions, the velocity in the x-direction appears as stationary bands, as shown in Figure 7. Since this does not accurately represent the behavior of the bubble column, simulations were then performed using a width of 100 cm, with no changes to the height or depth.

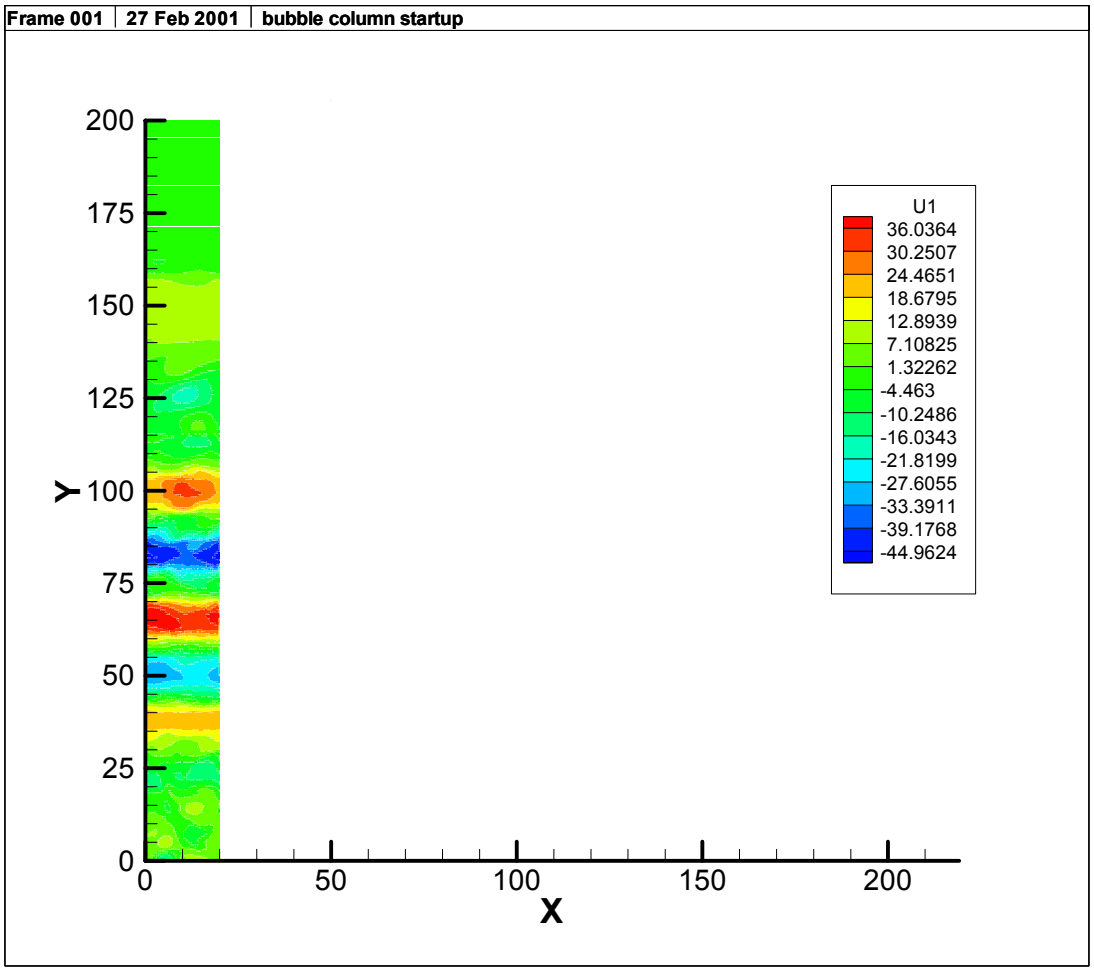

Figure 7 Contour Plot of Water Velocity in the X-Direction at t = 10 seconds

An obstacle involved in performing the 100-cm wide, 3D simulations is the length of time necessary for a sequential simulation. This could be improved by using a parallel CFDLIB code for simulations using periodic boundary conditions. Currently, there is no provision within the code for parallelization for use with periodic boundary conditions. Work began with consultants at the ISU high-performance computing facility to attempt to adapt the code for parallel use.

A possible work-around investigated this quarter was to utilize free-slip boundary conditions along the column walls. The parallel version of CFDLIB does work for this boundary condition. Simulations for both periodic boundary conditions and free-slip boundary conditions were performed using the conditions listed in Table 1. Comparisons were then made between the two types of boundary conditions. Examples of the results for this study are illustrated in Figures 8-11.

Table 1 Simulation Conditions

Column height	200 cm
Column width	100 cm
Column depth	2 cm
Bubble diameter	1.5 mm
Inlet superficial air velocity	2 cm/s
Initial water volume fraction, 0 cm to 40 cm height	1.00
Initial water volume fraction, 40 cm to 80 cm height	0.75
Initial water volume fraction, 80 cm to 120 cm height	0.50
Initial water volume fraction, 120 cm to 160 cm height	0.25
Initial water volume fraction, 160 cm to 200 cm height	0.00

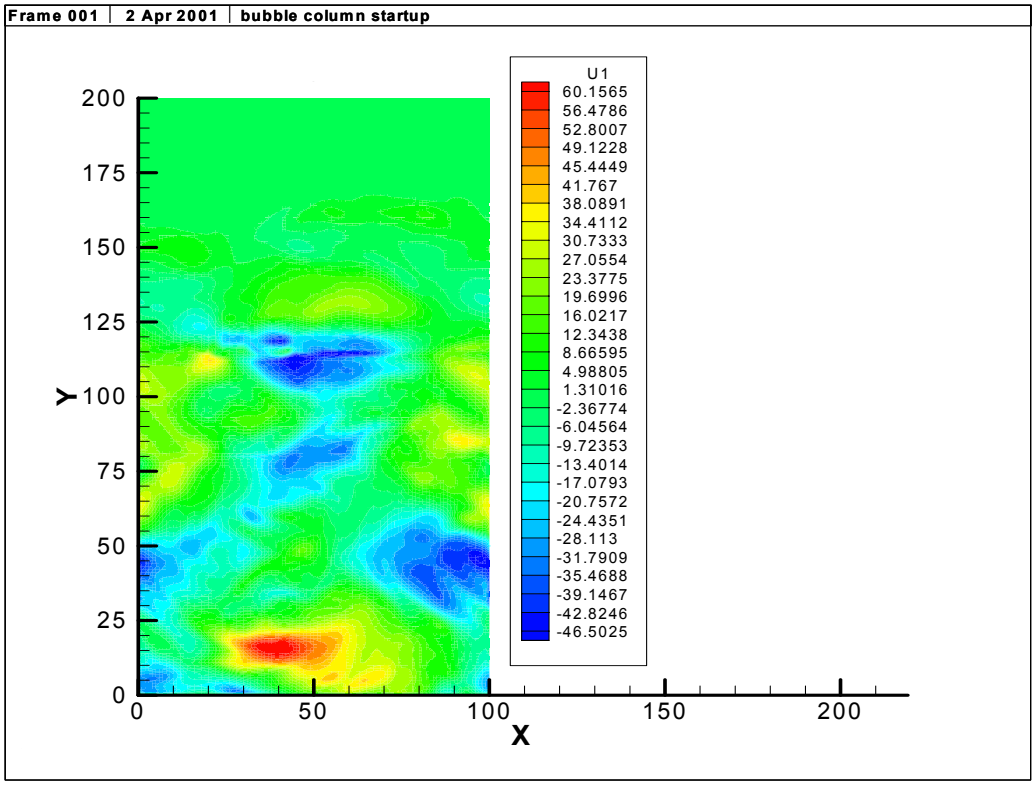

Figure 8 Contour Plot of Water Velocity in the X-Direction at t = 10 seconds with Periodic Boundary Conditions

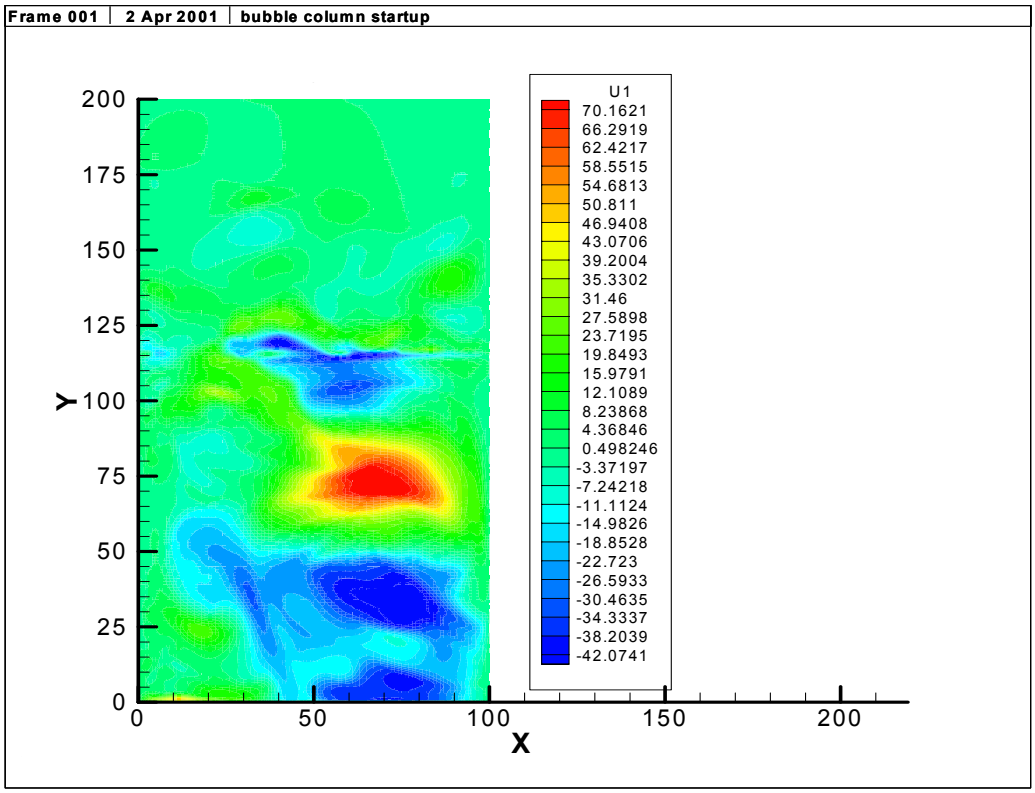

Figure 9 Contour Plot of Water Velocity in the X-Direction at t = 10 seconds with Free-Slip Boundary Conditions

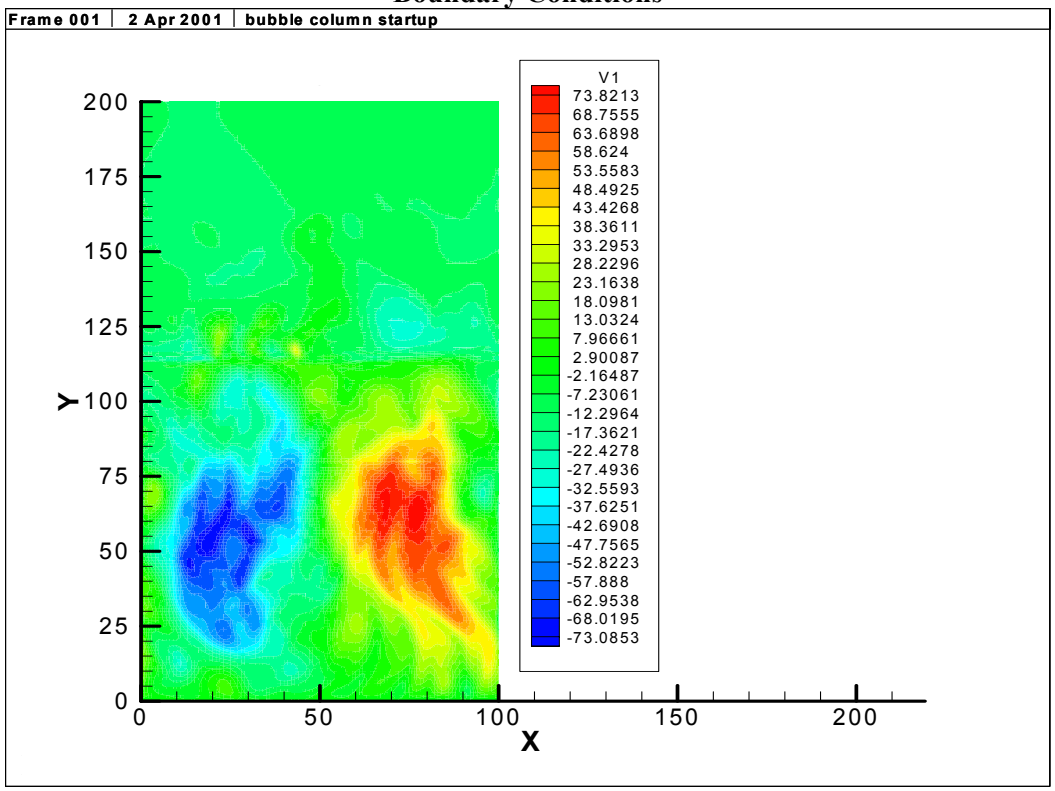

Figure 10 Contour Plot of Water Velocity in the Y-Direction at t = 10 seconds with Periodic Boundary Conditions

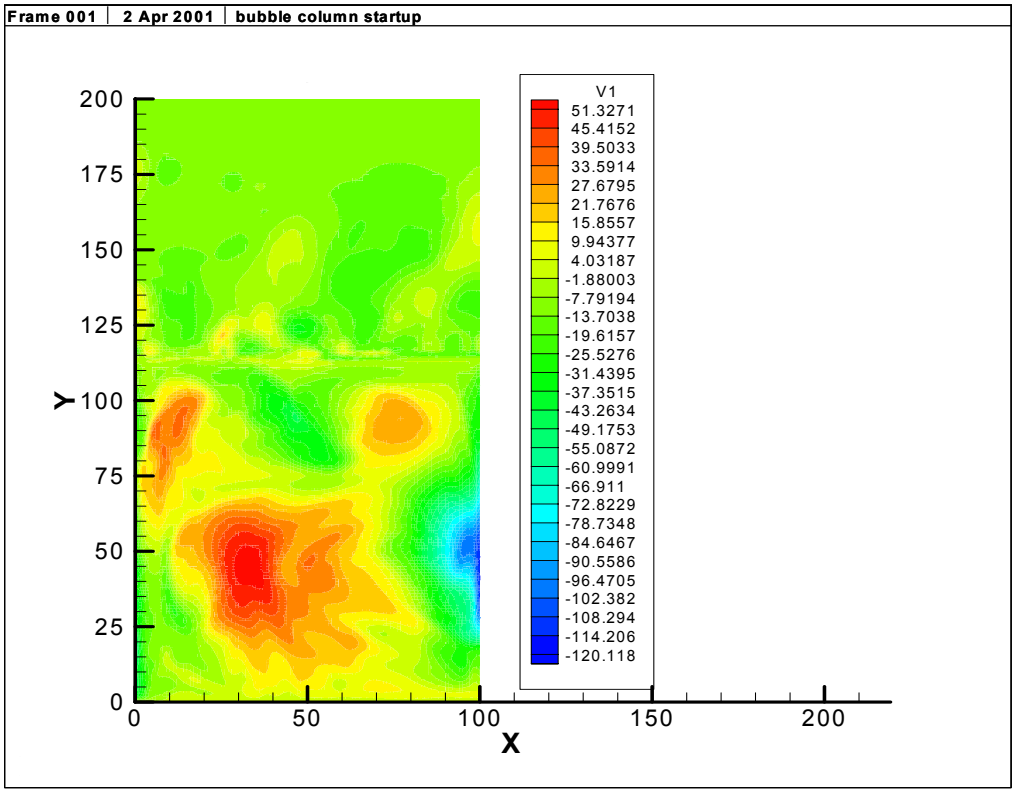

Figure 11 Contour Plot of Water Velocity in the Y-Direction at t = 10 seconds with Free-Slip Boundary Conditions

Figures 8 and 9 compare the differences in horizontal (x-direction) water velocity profiles for periodic and free-slip boundary conditions. For periodic boundary conditions, the highest magnitudes were observed at the walls at lower column heights, and as height increased, the higher velocities tended to occur in the center of the column. However, over time there should be no preferential location for high/low velocities. For free-slip boundary conditions, velocity magnitudes tended to be always highest in the center of the column.

Figures 10 and 11 compare the differences in vertical (y-direction) water velocity profiles for periodic and free-slip boundary conditions. The periodic boundary condition simulation resulted in high upward velocities along the right side of the column and high downward velocities on the left side of the column. Again, over time, there should be no preferential location. The free-slip boundary condition simulation resulted in high upward velocities always toward the center of the column. Velocity profiles in the z-direction were nearly the same for both types of boundary conditions, and had very low magnitudes.

The water volume fractions appeared to be more dispersed for the periodic boundary conditions, as shown in Figures 12 and 13. This is a strong indication that the characteristic length scales of the flow can be strongly influenced by the choice of the boundary conditions (in addition to the grid resolution).

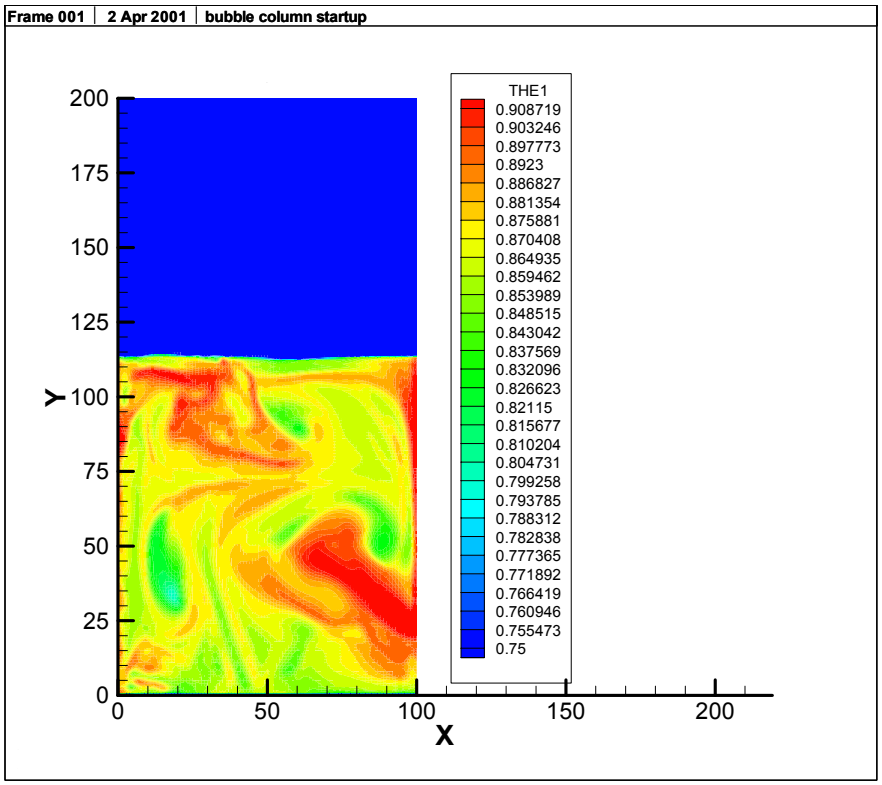

Figure 12 Water Volume Fraction at 10 seconds with Free-Slip Boundary Conditions

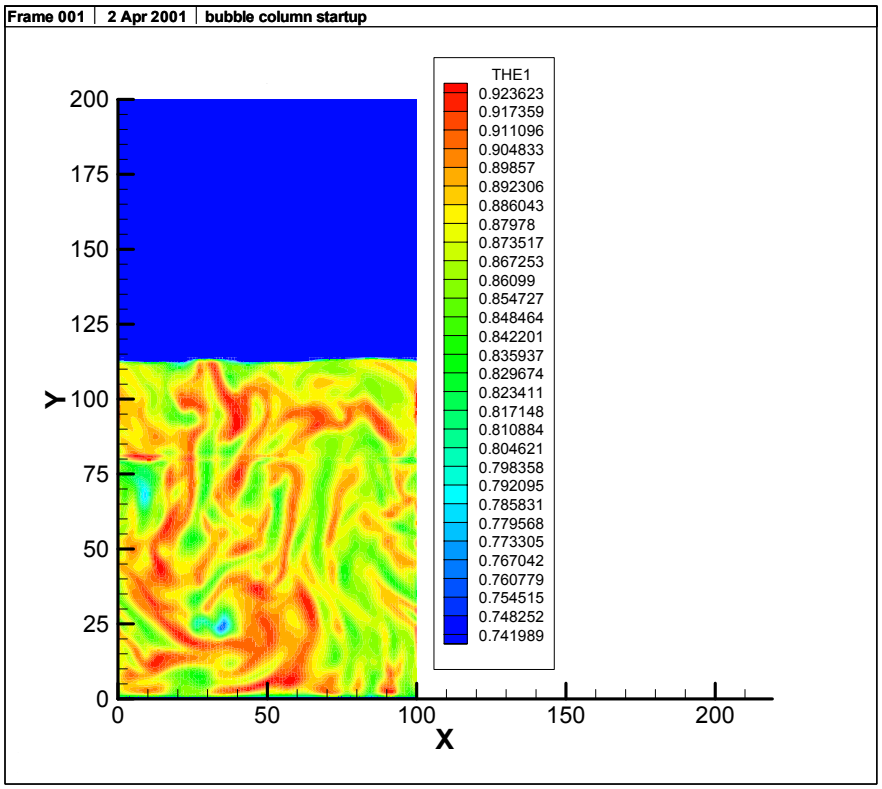

Figure 13 Water Volume Fraction at 10 seconds with Periodic Boundary Conditions

The effects of free-slip boundary conditions are best observed at locations a distance from the column walls. Simulations for this condition used a column depth of 2 cm, which may be too small a distance to properly utilize this type of boundary condition (at least with a 1-cm grid).

Future Work

Plans for the next quarter include simulations for longer times (i.e., 20-30 seconds) to collect data for time-averaged quantities. Future simulations will also include setting an initial volume fraction of water equal to 1.0 up to a height of 150 cm, and an initial volume fraction of water equal to zero between 150 and 200 cm, to see if changes in the initial water volume fraction affect the flow patterns observed in simulations.

Due to the high cost of 3D simulations, we plan to test the validity of 2D simulations with periodic boundary conditions for representing the time-averaged statistics. This will be done by running a single "high-resolution" 3D simulation of sufficient length to collect statistics, and comparing these results to 2D simulations. In order to carry out these calculations, we plan to purchase an 8-processor SMP computer (Sun Fire 3800) during the next quarter. The availability of this machine should greatly increase the range of simulations that we will be able to run.